Title: **Payload Preliminary Design Description**

DRD No.: LISA-MSE-DD-0001, Issue 1, rev1

Prepared by:	Marcello Sallusti	Date:	01/04/2009
Checked by:			
Approved by:			

Distribution: See Distribution List

Change Record

Issue	Date	Section	Description of Change	Release

Table of Content

1 INTRODUCTION

The Laser Interferometer Space Antenna (LISA) is a cooperative mission between ESA and NASA. Its goal is to detect gravitational waves created by astrophysical objects and events, such as ultra-compact galactic binaries and the merger of super-massive black holes, which can only be detected by a space-based observatory. The existence of gravitational waves has long been predicted and their unambiguous detection would open up a new field of astronomy based on non-electromagnetic observations.

Gravitational waves will be observed by LISA using laser interferometry, implemented in a constellation of three identical spacecraft. Each spacecraft will contain two reference targets, known as “proof masses”, each of which acts as the end mirror of a single-arm interferometer. By having the three spacecraft flying in an equilateral triangular formation, three semi-independent two-arm laser interferometers can be formed (Figure 1-1). The passage of gravitational waves will be measured by observing combinations of the movements of the proof masses, and thus arm length changes.

For the unambiguous detection of gravitational waves great pains must be taken to avoid perturbations to the proof masses from other sources, such as spacecraft manoeuvre, solar radiation pressure, magnetic fields, the outgassing environment, and the gravity field from the spacecraft. The Level 1 (system) requirement is to reduce non-gravitational accelerations.

The Measurement Band Width (MBW) over which LISA operates will be 0.1 mHz to 0.1 Hz, with the goal to be able to operate in an extended band from 0.03 mHz to 1 Hz. This MBW is where much of the most interesting gravitational wave sources are emitting, and is directly complementary to a number of planned ground-based interferometers (LIGO, VIRGO, TAMA 300 and GEO 600) that will observe gravitational waves over the higher frequency regime (10 – 1000 Hz). These ground-based observatories will be unable to access the low frequency gravitational wave domain addressed by LISA due to intrinsic sensitivity limits caused by the Earth’s own gravitational field, seismic activity, and other unavoidable environmental disturbances.

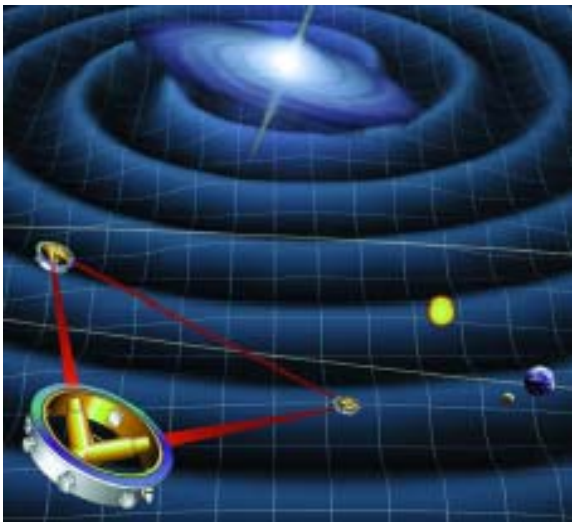

Figure 1-1: LISA constellation (artist’s view).

2 SCOPE

This document gives a brief overview of the major elements Payload as defined during the Mission Design Review (MDR).

It describes the general payload design concept and give some details for the elements that are the most critical for the achievement of the mission requirements or that are characterized by the tightest requirements.

It does not include the description and the results of the mechanical and thermal design. These topics, together with a more extensive description of the PL elements are described in full detail in RD4 and in the other project specific documents.

3 DOCUMENTS

3.1 Applicable Documents

AD	Doc. No.	Title
	NA	

3.2 Reference Documents

RD	Doc. No.	Title
01	LISA-ASD-TN-1002	LISA Measurement Performance
02	LISA-ASU-TN-4001	Mission Analysis
03	LISA-ASD-BR-5002	System Parameters and Error Budgets
04	LISA-ASD-DD-3001	Payload Preliminary Design Description

4 Scientific Requirements and Payload Concepts

The LISA space segment will consist of three spacecraft flying in three independent orbits. The orbits are designed such that, without the need for station keeping, form a quasi-equilateral triangular formation in an Earth-trailing/leading orbit at some 20 degrees offset from the Earth (see Figure 4-1). Each of the three identical spacecraft carries a measurement system consisting of two free-flying test masses (that will undergo displacement due to the passage of gravitational waves) with associated laser interferometers and electronics. Any two of the three arms of the formation form a Michelson type interferometer, which is realized by sending infra-red laser radiation back and forth between the individual s/c payloads. Low frequency gravitational waves will be detected through measurement of differential changes in the optical path lengths of the two interferometer arms.

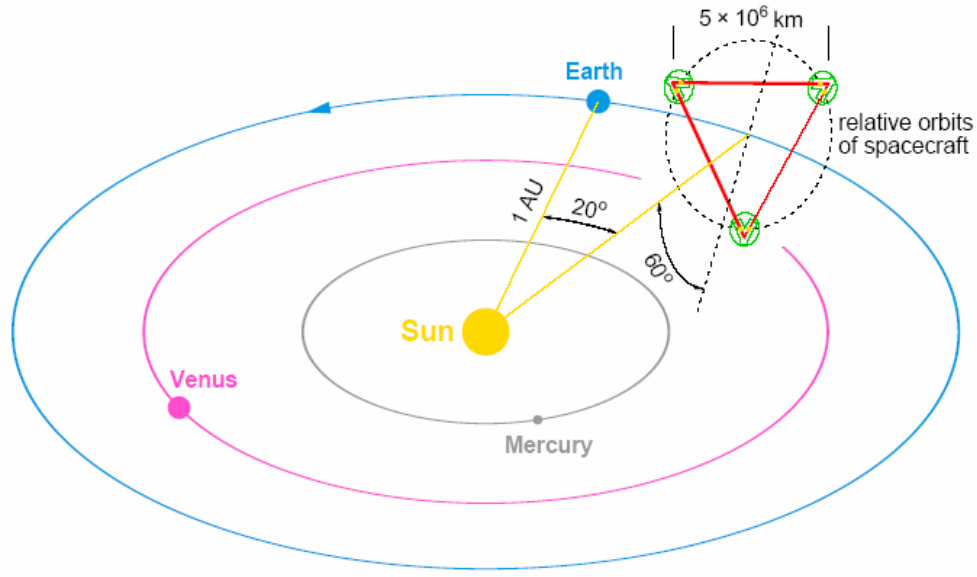

Figure 4-1: Schematic diagram of the LISA operational configuration. The plane of the LISA triangle is tilted by 60 degrees out of the ecliptic. The centre of the triangle moves around the Sun, in the same orbit as the Earth, but either leading or trailing.

4.1 Payload Requirements

The top level requirement for the LISA payload is that it has to enable gravity wave detection at low frequencies with the strain sensitivities shown in Figure 4.1-1 [RD-01]. The values are given in terms of a spectral density of the gravitational strain measurement accuracy, where the strain sensitivity *h* is a measure for the gravitational wave amplitude and is proportional to the relative arm length change:

$$h = 2\frac{\delta L}{L}$$

Here, *L* is the arm-length expressed in [m] and δL the arm-length variation in [m/√Hz]. From the above equation and taking the scientific requirement shown in Figure 4.1-1 below, the LISA interferometric measurement system has to provide an absolute accuracy in the range of **18 pm/√Hz** for a single arm laser link, given an arm length *L* of 5 million kilometers.

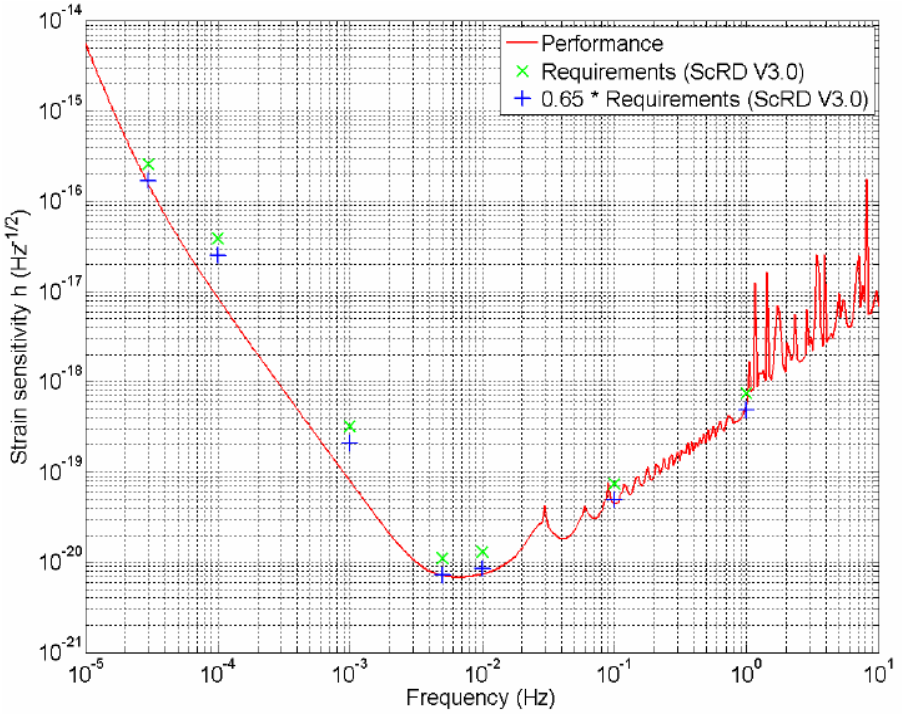

Figure 4.1-1: Required gravitational waves strain sensitivity.

Frequency (Hz)	**Strain sensitivity (as per ScRD requirements, $1/\sqrt{Hz}$)**	**Design Strain sensitivity requirement (with 35% system margin, $1/\sqrt{Hz}$)**	**Comments**
3×10^{-5}	2.6×10^{-16}	1.69×10^{-16}	
1×10^{-4}	3.9×10^{-17}	2.54×10^{-17}	
1×10^{-3}	3.2×10^{-19}	2.08×10^{-19}	
5×10^{-3}	1.1×10^{-20}	7.15×10^{-21}	
1×10^{-2}	1.3×10^{-20}	8.45×10^{-21}	
1×10^{-1}	7.5×10^{-20}	4.87×10^{-20}	
1	7.5×10^{-19}	4.87×10^{-19}	

Table 4.1-1: *LISA measurement sensitivity requirements;*

The accurate determination of arm length variations is complicated by the fact that the shape of the constellation of 3 spacecrafts undergoes residual seasonal changes, which cannot be completely removed by orbit optimization. These changes not only affect the nominal 60° angle between the lines of sight, but also the so called point-ahead angle, which describes the offset between received and transmitted beam for each individual s/c. This offset is required to account for the SC motion during the comparatively long travel time of the laser light to the respective remote s/c, which is calculated to be approximately 16.7 s.

Plots for the variation of the angle between the LOSs and the point-ahead angle, derived for the current status of orbit optimization [RD-02], are given in Figure 4.1-2 and Figure 4.1-3, respectively. The amplitudes of the variation of the LOS angle (±1°) and the out-of-plane point-ahead angle (±6 µrad) are so large that an active compensation is required. For the in-plane point-ahead angle variation of less than ±0.1 µrad, no accommodation is considered necessary, as it stays an order of magnitude below the diffraction limited beam divergence of about ±1.9 µrad for the TX beam in the far field.

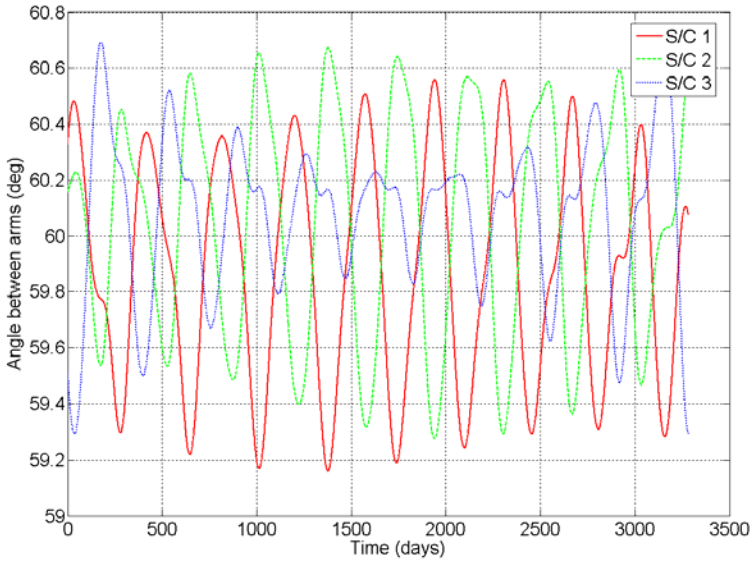

Figure 4.1-2: Predicted angle between the interferometer arms for the baseline science orbit [RD-03].

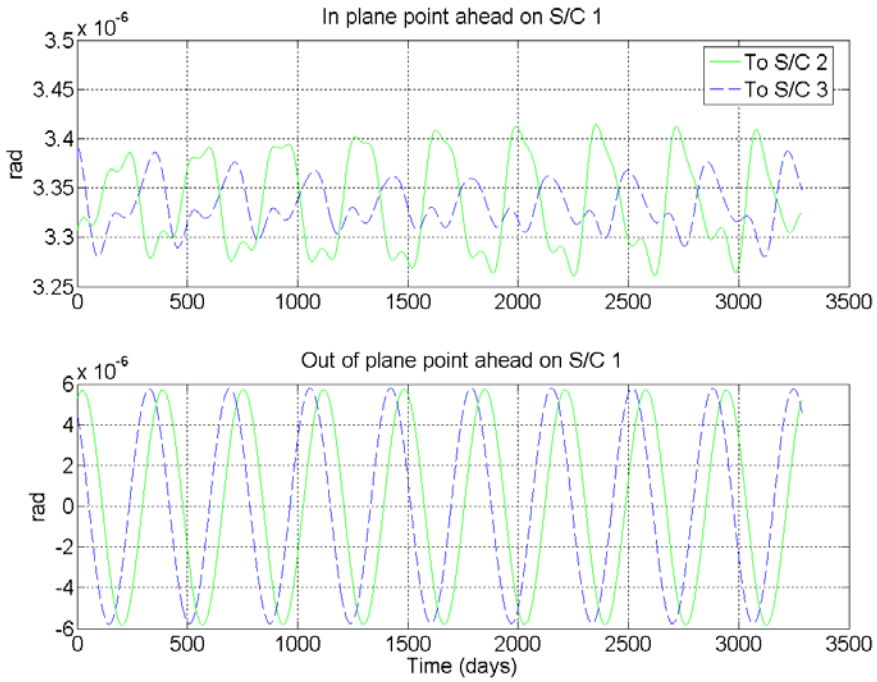

Figure 4.1-3: *In plane and out of plane point-ahead angles, as calculated for s/c 1. The amplitude of the variation is also representative for the other two spacecrafts.*

4.2 Payload Metrology Concept

In science operation, each LISA spacecraft will establish transponder-like laser links to the other two spacecraft in the constellation, so that each interferometer arm is formed by two counter-propagating laser beams. For this purpose, each spacecraft contains two virtually identical Moving Optical Subassemblies (MOSAs), which serve their individual interferometer arm and optically connect with their remote counterpart,

Each MOSA, as illustrated in Figure 4.2-1, contains as main elements an Optical Bench (OB), a Gravitational Reference Sensor Head (GRS Head) containing the free floating Proof Mass constituting the interferometer end, and a 40 cm telescope (TS). This product structure and the intended implementation is described in some detail in this document.

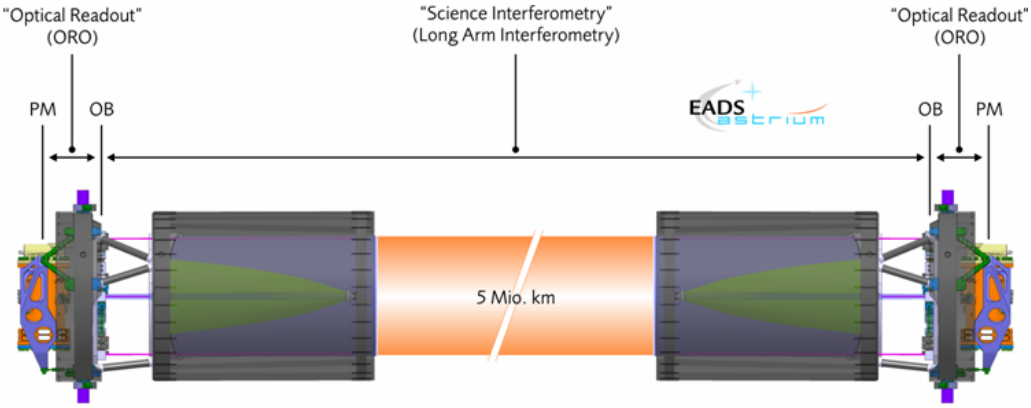

Figure 4.2-1: Configuration of one LISA interferometer arm in the so-called "strap-down architecture".

In the so-called **strap-down architecture**, the optical detection of fluctuations in the distance between the two poof masses of each interferometer arm is separated into three steps:

- Local Proof Mass to Local Optical Bench
- Local Optical Bench to Remote Optical Bench
- Remote Optical Bench to Remote Proof Mass

The individual interferometric measurements on board the three LISA spacecraft are combined in ground processing using a procedure known as Time Delay Interferometry (TDI) to extract gravitational wave signals. TDI basically forms a virtual equal-arms interferometer from all the metrology data recorded in the constellation. As with all interferometric measurements, the principle measurement is a differential displacement along two or more arms of the constellation for timescales in the LISA measurement band.

The measurements are performed using **polarizing heterodyne interferometry** with two independent active laser systems on board each spacecraft (Figure 4.2-2). Each laser feeds one optical bench and the corresponding interferometer arm. The laser light is transmitted to the remote spacecraft through the same telescope that receives the incoming beam. Orthogonal linear polarizations are utilized to perform the send/receive multiplexing. The transmit and receive beams traverse the telescope optics at slightly different angles because of the point ahead angle required by the relative motion of the spacecraft and the finite light travel time. The point ahead angle is discussed in Section 5.2.2.2 of this document

The two lasers on board are operated at slightly different optical frequencies and shared between the two optical benches with a fiber link to generate heterodyne signals between 5 and 20 MHz. The applicable heterodyne frequencies are defined by the range of possible Doppler shifts from the relative motion of the three LISA spacecraft. Therefore, each interferometer must be capable of handling any heterodyne frequency in this range. The phase measurement itself is performed with a digital phasemeter using phase locked loops referenced to an Ultra Stable Oscillator (USO).

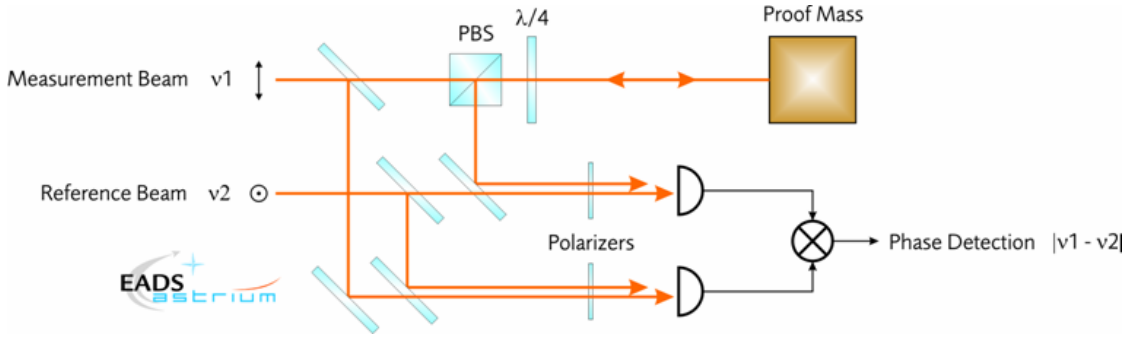

Figure 4.2-2: Basic principle of polarizing heterodyne interferometry for the example of the Proof Mass Optical Readout (ORO).

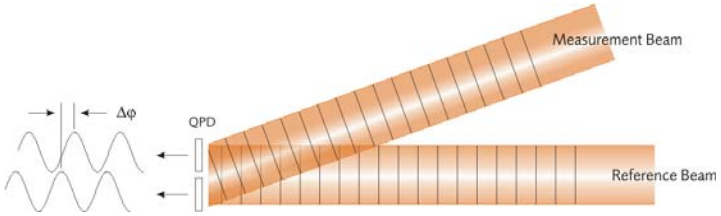

Figure 4.2-3: Principle of Differential Wavefront Sensing.

The main science interferometer employs **Differential Wavefront Sensing** (DWS) for the detection of wavefront tilt of the measurement beam with respect to the reference beam in addition to longitudinal phase shifts. This is accomplished by combining heterodyne interferometry with a spatially resolved phase measurement through the use of quadrant photodiodes (QPDs). The signals obtained from the individual quadrants show relative phase shifts, depending on the spatially dependent phase difference between reference and measurement beam, from which the relative wavefront tilt can be inferred with high accuracy (Figure 4.2-3).

5 Payload Functional Architecture

5.1 Overall Payload Architecture

The LISA Payload as part of the LISA Spacecraft is subdivided into several subsystems which are shown in Figure 5.1-1 below. Globally seen, the Optical Assembly Subsystem (OAS) is the part containing all optical, mechanical and sensing components for the measurement of the optical path strain. This includes also the Gravitational Reference Sensor (GRS) Head containing the Proof Mass that constitutes the reference end of the interferometer arm. Despite being hosted in the OAS, the GRS Head belongs to the GRS Subsystem, which comprises also all the related sensor electronics. All the components and the electronics units necessary for the interferometric metrology are grouped in the Phase Measurement Subsystem (PMS). The Laser Subsystem (LS) produces the light necessary to actually realize the interferometer and the Diagnostics Package (DP) provides ancillary measurements used to better characterize the environmental conditions in which data are taken.

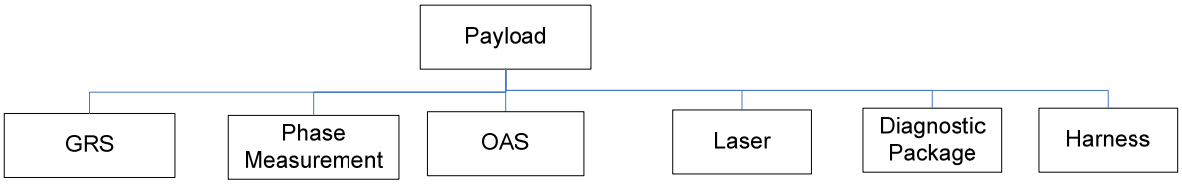

Figure 5.1-1: Highest Layer of Payload Subsystems

5.2 Optical Assembly Subsystem (OAS)

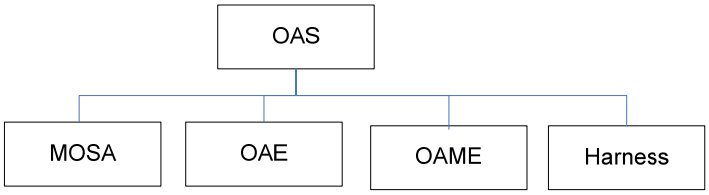

Figure 5.2-1: *Breakdown of the Optical Assembly Subsystem*

Practically, the LISA Optical Assembly Subsystem consists of two Movable Optical Sub-Assemblies (MOSA), oriented at a nominal angle of 60° and associated electronics. Each MOSA serves one of the two adjacent interferometer arms and is rotated as a whole within the constellation plane in order to cope with the "breathing angle". In order to provide redundancy capabilities, each Movable Optical Sub-Assembly is fed by two independent laser systems operated in cold redundancy. The Laser switching mechanism is located on

the optical benches. The laser system of one MOSA is phase correlated via a backside fiber link to the one of the other MOSA, and serves also as local oscillators on the other optical bench for the heterodyne phase detection of incoming light beam. The Payload electronics and laser assemblies are distributed throughout the spacecraft.

The Movable Optical Sub-Assemblies contain the complete optical system of LISA (telescope, optical bench, mirrors and lenses), the mechanical structure holding together the MOSAs components, the optical assembly tracking mechanisms (OATM) and the launch locks (LLD).

The OAME and OAE are electronics boxes supporting respectively the OAS mechanisms and the active optical units.

The OAME (optical assembly mechanisms electronics) contains the actuation and sensing electronics for the Optical Assembly Tracking Mechanism (OATM), the Refocussing Mechanism (ReM), Point Ahead Angle Mechanism (PAAM) and Fibre SWitches (FSW) which are hosted on the Optical Bench. Note that the point ahead mechanism may use a more precise sensor signal representing the actual pointing direction that is available from optical metrology.

The OAE (optical assembly electronics) contains the power supply for the photodiodes' pre-amplifiers and it allows to selectively supply only those amplifiers needed in a given redundancy configuration. Also detector housekeeping signals are acquired (e.g. dc current representing I/O-power) which might be needed for health monitoring. Furthermore the OAE contains the support and interfacing electronics for the CCD sensors used for spatial attitude acquisition.

The optical assembly harness is part of the optical assembly subsystem as well as a dedicated passive thermal insulation.

5.2.1 Moving Optical SubAssembly (MOSA)

The heart of the LISA payload are the Moving Optical Subassemblies (MOSAs). Each MOSA implements an optical transceiver for one optical link to a distant spacecraft and consists of MOSA Structure, the Telescope Subsystem, Optical Bench Subsystem, GRS Head and MOSA Thermal Shield.

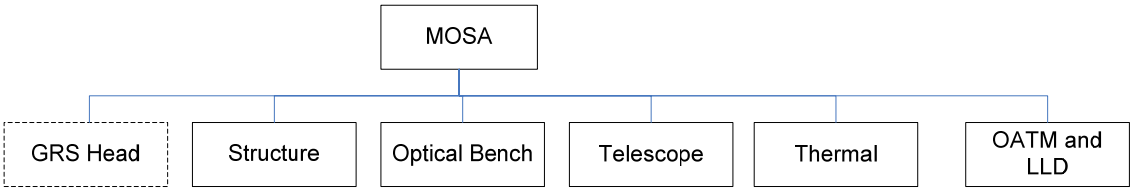

Figure 5.2-2: *Breakdown of the Moving Optical Subassembly*

"Movable" in this context refers to rotation around an axis perpendicular to the plane defined by both MOSAs, which is required to compensate for the seasonal changes in the angle in the plane of the constellation between the two adjacent line-of-sights.

Mechanically, a 40 cm aperture telescope is isostatically mounted to a CFRP structure which also contains an optical bench made of Zerodur® and a gravitational reference sensor. The telescope directs the incoming

light onto a folding mirror on the optical bench. On there, the light is processed as described in the dedicated section on the optical bench design.

The optical bench is oriented perpendicular to the telescope axis with the optics facing the telescope side, which allows for a compact and mass efficient optical assembly design. It is mechanically supported by three isostatic mounts and maximally decoupled from external forces. In particular, the Gravitational Reference Sensor assembly mechanical transfer function is directly interfaced to the central support ring. The optical bench carries some of the telescope optical components (including the focus adjustment mechanism, ReM), the transmit and receive interferometer optics and relevant fiber launcher, the CCD sensor for the laser link initial acquisition, the point-ahead angle mechanism, a local laser phase correlator, and a dedicated laser interferometer for precision sensing of proof-mass axial position and lateral attitude (optical readout). Opto-mechanical switches are foreseen to perform redundancy switching for all optical signals which are delivered to the MOSAs by optical fibres (laser input and back-fibre between the two MOSAs).In total each MOSA provides 29 different detector signals carrying beat notes of heterodyne interferometers. Of these, 20 signals are simultaneously active while 9 signals provide cold redundancy. The subsystems are further described below.

All elements are thermally isolated in order to secure thermoelastic stability. To further ensure disturbance minimization, an extremely stable thermal environment is required, with no active thermal elements able to induce mHz disturbances at the payload interface. Effectively this requirement drives the payload thermal environment to be well decoupled from both solar radiation and in turn from the SC structure itself. At Spacecraft level, a sunshield is provided to protect the spacecraft from the sun, and at payload level, the carbon composite structure can be coupled with radiators to provide passive thermal control.

In addition ancillary interferometers can be optionally included in the MOSAs and are shown in figure 5.2-4 just for reference. These serve for measurement of PAAM effective pointing and pathlength impact as well as transmitted wavefront variation ('"optical truss"). For the purpose of the Optical Truss measurement, a small fraction of the laser light leaving the telescope is picked off at three locations on the telescope inner housing on the secondary mirror ring, separated by 120°, where photodiodes are mounted. This light is mixed with a collimated local oscillator laser beam launched from the optical bench, to yield a heterodyne signal at frequencies in the range 5 - 20 MHz. Together with a reference signal generated on the optical bench, this signal allows for detection of picometer pathlength variations in the complete path from optical bench to telescope exit.

The structural implementation of this optical layout can be seen in Figure 5.2-3.

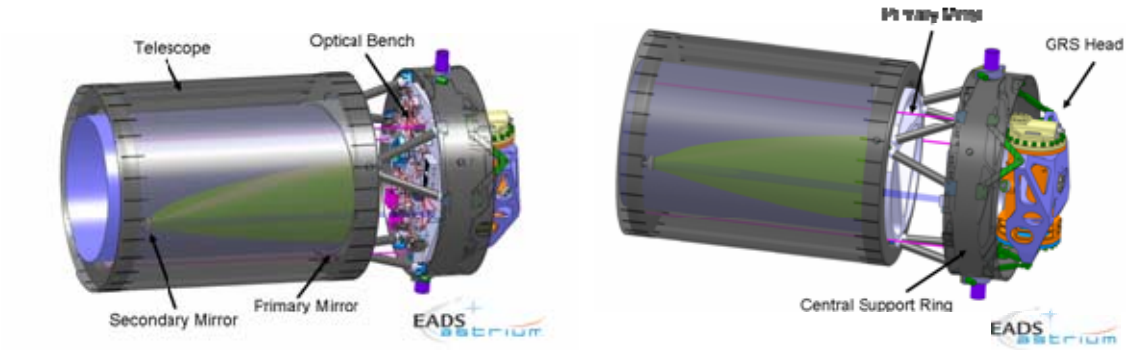

Figure 5.2-3: *Moving Optical Assembly (MOSA) Layout*

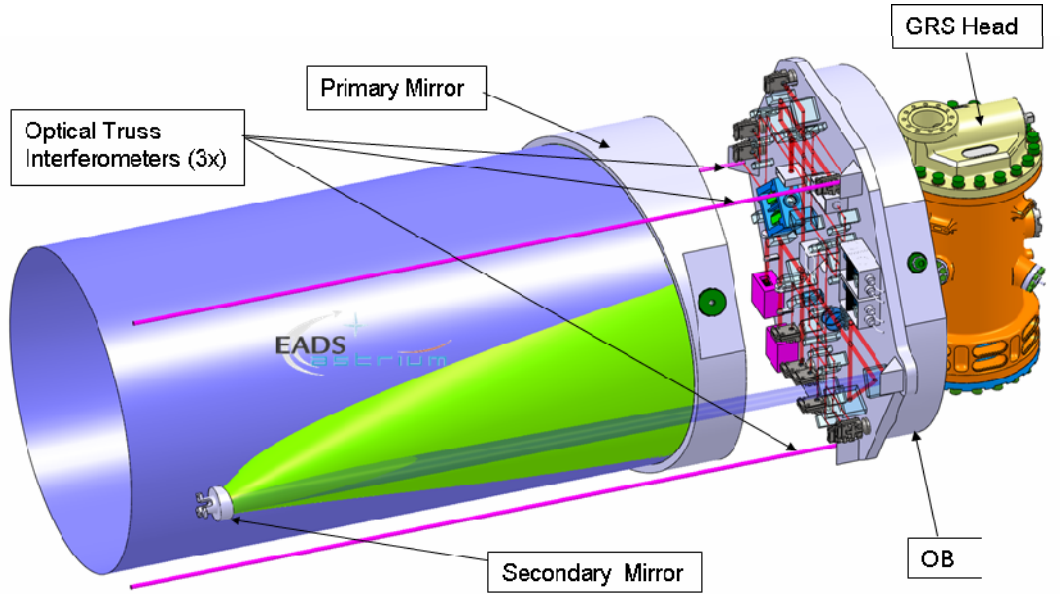

Figure 5.2-4: *Overview of MOSA optical layout - front view*

5.2.1.1 Telescope

The telescope design is characterized by its optical properties from its accessible internal pupil to its virtual external pupil and by sufficient field-of-view for point-ahead angle accommodation. In the current design the diameter of the internal pupil is 5 mm and that of the external pupil is 400 mm. The external pupil is virtual as it shall be located at the position of the Center of Mass of the Proof Mass inside the Gravitational Reference Sensor, which is actually accommodated behind the telescope.

Further guidelines considered for the design have been:

- Optical performance (< λ/30 rms wavefront error over required FoV)
- Intrinsic avoidance of stray light
- Avoid extremely decentered apertures
- Back-scatter from the lenses being minimized
- Accessibility of the exit pupil for positioning of the PAA Mechanism
- Minimum number of elements with overall compact dimensions
- Standard mirror manufacturing prescriptions

Given the above mentioned design guidelines, the most convenient telescope design resulted in an off-axis 2 mirror telescope. The basic functional elements of the Telescope Subsystem are illustrated in Figure 5.2-5 (the back optics will be hosted on the Optical Bench) and the design characteristics of the telescope are summarized in Table 5.2-1. The main optical elements in the telescope are considered to be the ocular system and the assembly of primary and secondary mirror.

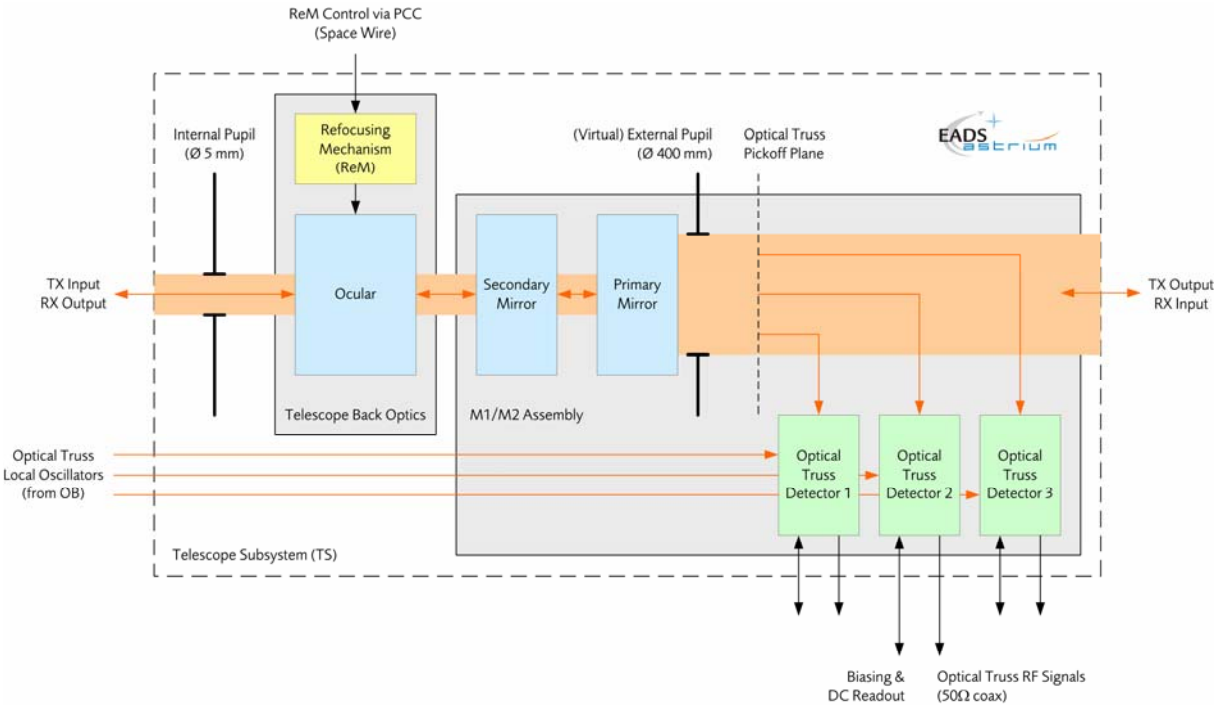

Figure 5.2-5: *Functional Architecture of the Telescope Subsystem.*

Telescope Design Fact Sheet	
Virtual Entrance Pupil	400 mm diameter, at PM location
Primary Mirror	Parabolic, 405 mm aperture
Secondary Mirror	Hyperbolic, 30 mm aperture
M1 – M2 Separation	596 mm
Ocular	2 spherical Fused Silica lenses
Total glass thickness	8.5 mm (< 40 mm required due to dn/dT effects)
Accessible Exit Pupil	5 mm diameter 203 mm after last element
Overall Magnification	80
Instantaneous FoV	±0.02° (±350 µrad) (about ±200 µrad FoV required on CCDs)
Design Wavefront Error	< λ/200 rms @ 1064 nm
Constellation	6 identical designs in constellation
Telescope Path Metrology	Optical truss, including wavefront tilt metrology.

Table 5.2-1: *Telescope Design Characteristics*

The telescope design provides an off axis ocular with decentred pupil aperture. The alignment of the exit pupil is corrected by the folding mirrors and the beam is collimated with a transmissive ocular lens arrangement system located on the optical bench. The ocular lenses are designed to fully suppress in-field (specular) back reflected light. They are assumed to have a 40 mm lens diameter and 18 mm useful aperture diameter.

This arrangement is not necessarily prescribed. However, an appropriate interfacing with the optical bench has to be realized, which will be subject of an extensive ICD, once in the implementation phase.

Along the same line, it is not absolutely required at this stage that the Refocusing Mechanism (ReM) acts on one or more elements in the ocular as in the current design, even though this is currently the more attractive solution. The major design driver for realization of the ReM is to achieve the required end-to-end wavefront quality while maintaining a pathlength stability on the picometer level. In particular the latter issue makes a set-and-forget actuation of a lens particularly attractive, since in this case any residual actuation noise would not directly impact the optical pathlength to first order.

The telescope configuration is illustrated in Figure 5.2-7 including calculated beam trains.

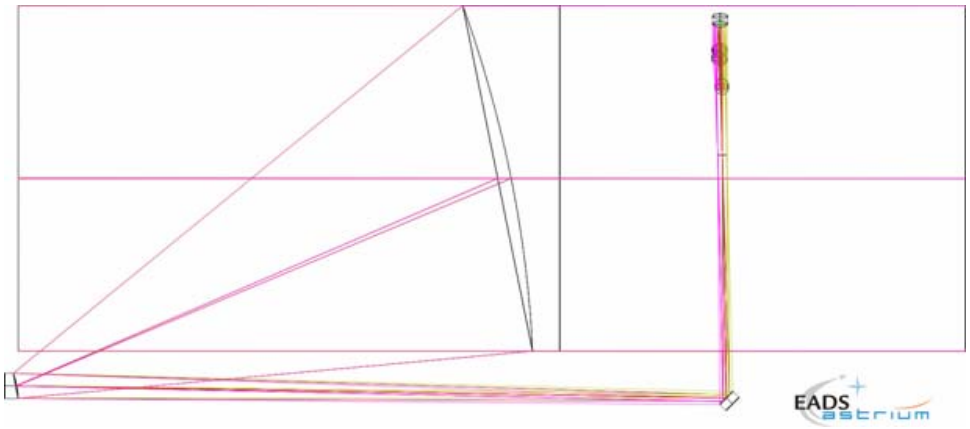

Figure 5.2-6: *Telescope Optical Path with Back Optics -Side View*

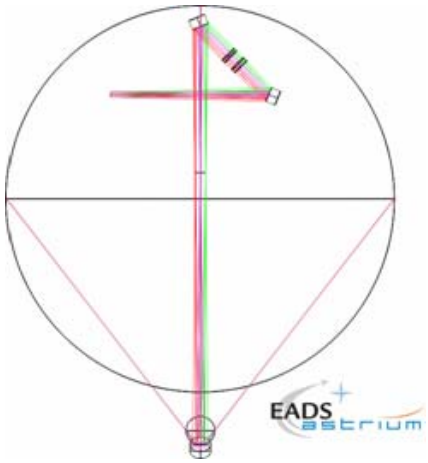

Figure 5.2-7: *Telescope Optical Path with Back Optics -Back View*

The Telescope optical components, in particular Optical Bench, M1, and M2 are considered to be manufactured from Zerodur. The Telescope mechanical part instead consists of three CFRP main structure parts, the M1 Support Ring, the M2 Support Ring and a Zero-CTE matched outer connection tube called Telescope Spacer. The Primary Mirror, equipped with glued Titanium Interface bushes, is isostatically mounted with the help of three CFRP-Isomounts separated by 120° which could be later directly connected to the OB Interface Ring. The outer M1 Support Ring is decoupled against the same connection points (front end of isostatic mounts) with the help of 3 flat CFRP-Isostatic mounts. These are glued to the inner side of the M1 Support Ring. The main outer dimensions of the TS is: diameter of 565 mm with a overall length of 740 mm (without Isostatic Mounts to Interface Ring and Thermal Hardware)

The telescope back optics is accommodated on the optical bench after a folding mirror.

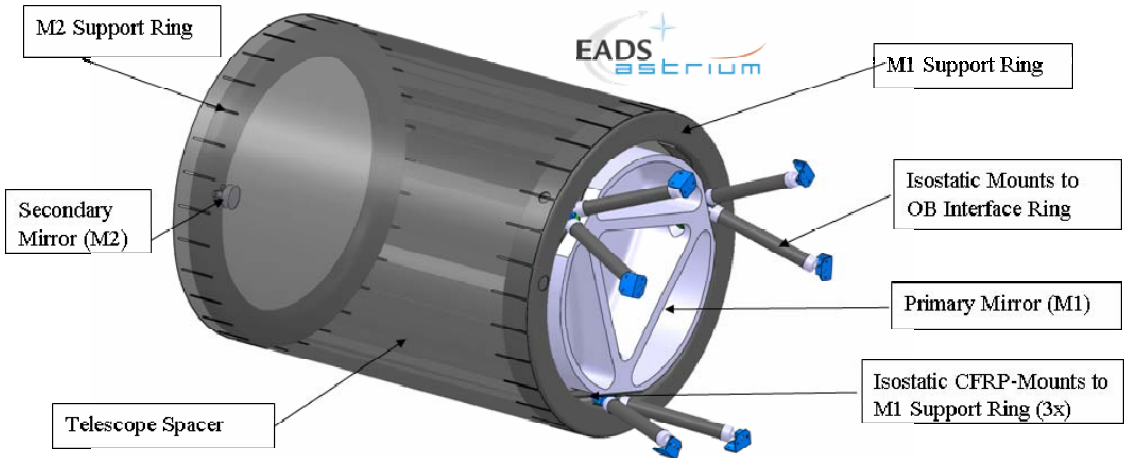

Figure 5.2-8: Telescope Subsystem with interfaces (IMs) to the Central Support Ring

Protection from stray light interference, also from the sun, is provided by appropriate baffling in the telescope as well as by a CFRP tube surrounding the complete movable part of the payload.

5.2.1.2 Optical Bench

The optical bench subsystem contains all elements that are needed for scientific interferometry. For this, the optical bench contains three interferometers, in accordance with the measurement principles described above: the main science interferometer, the optical readout interferometer, and the reference interferometer. Additional detectors are the PAAM metrology interferometers, power monitor diodes for the transmitted laser beam, CCDs for initial acquisition of the laser beam from the remote s/c, and a detectors belonging to the reference cavity assembly.

An overview of the functional architecture of the LISA Optical Bench is given in Figure 5.2-9. It defines the optical interfaces as well as the beam routing between the main opto-mechanical and opto-electronic elements located on the Optical Bench. Each optical bench manipulates a total of three continuous wave, narrow linewidth, slightly separated laser frequencies near 1064 nm (identified by the three different colors in the figure).

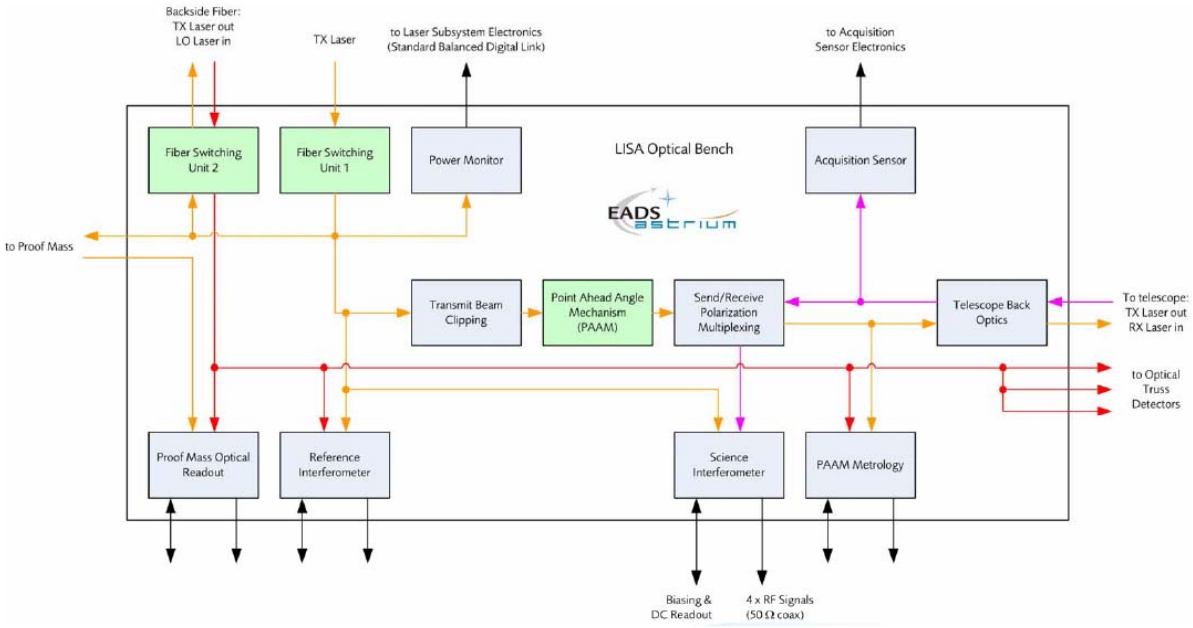

Figure 5.2-9: *Functional Architecture of Optical Bench - with Optical Path*

The bench baseplate is a lightweight Zerodur structure, which provides the basis for a sufficient dimensional stability of all relevant optical path lengths in the complete science chain. Hydroxide catalysis bonding is used to mount the optical elements, made from Fused Silica, on the polished surface of the optical bench. The OB will be isostatically mounted with the help of three 120°arranged CFRP-Isomounts in the outer very stiff designed CFRP Interface Ring.

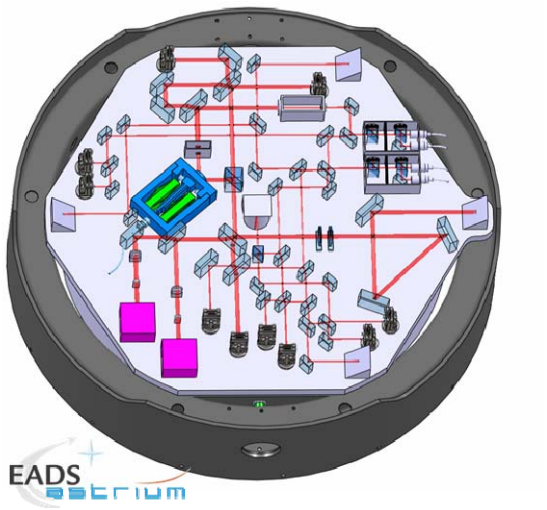

Figure 5.2-10: Optical Bench Subsystem mounted to CFRP-Interface Ring

Figure 5.2-11 shows the layout of "optical bench 1", from which the local oscillator "LO1" beam is transmitted, and for which the "LO2" beam (local oscillator of the other optical bench) is delivered via the backside fiber link. The main portion of the LO1 light is directed over the PAAM actuator and towards the telescope for transmission to the remote s/c. Demultiplexing of the incoming beam is realized with a polarizing beam splitter where the received light is mixed with LO1 from the other optical bench. LO1 is also made available to the other optical bench by routing a small fraction of its power to a fiber connecting the two optical benches. It transports both LO1 and LO2 in opposite directions in order to reduce common mode errors.

The optical readout of the proof-mass position and attitude with respect to the optical bench employs polarizing heterodyne interferometry in combination with differential wavefront sensing. LO1 is bounced off the front proof mass surface and subsequently mixed with LO2 to provide the heterodyne signal.

The optical bench contains a LO1 – LO2 reference interferometer for phase cancellation. It defines the phase reference point for all interferometers on the optical bench, whose temperature stability guarantees sufficient phase correlation between the individual channels. The LO1 – LO2 beat signal will be directly used for demodulation of all other heterodyne signals to cancel out common mode errors.

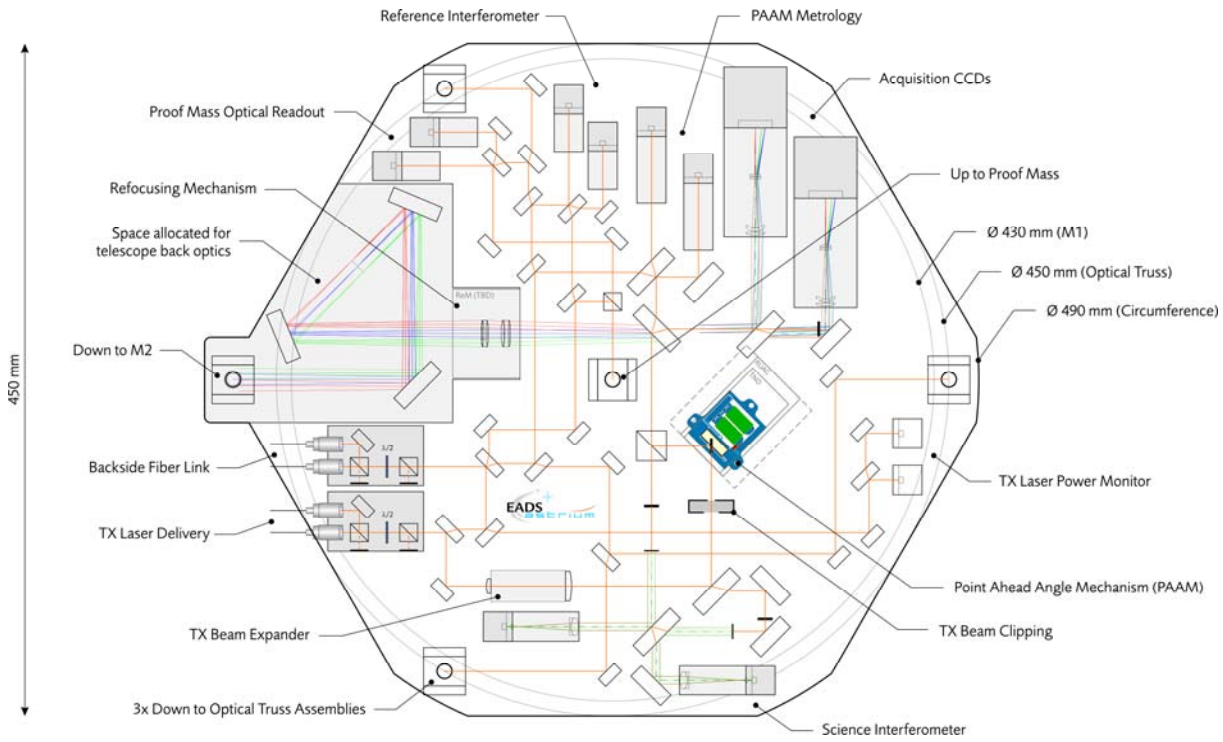

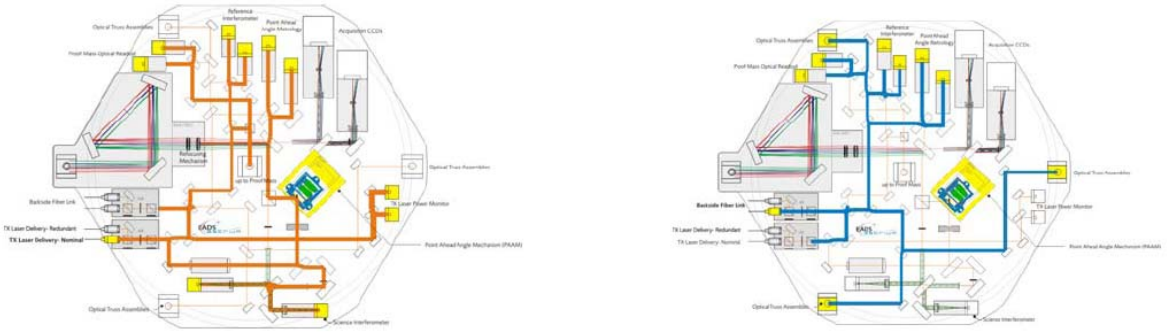

Figure 5.2-11: Optical bench layout and beam routing

Optical Bench and Metrology Fact Sheet	
OB Layout	Single-sided Optical Bench 2 x 3 identical benches (differ by 1 waveplate) Isostatically mounted, free of external loads Vertical orientation, parallel to M1 ∅ 580 mm
PM Metrology	Single-sided ORO 1 translational DoF 2 rotational DoFs
PAAM Configuration	PAAM in transmit path Dedicated optical tilt & piston metrology.
LO distribution	Backside fiber link

Figure 5.2-12: *Optical Bench and Metrology Fact Sheet*

The optical imaging for the complete system is designed such that the PAA actuator, the proof mass surface, and all RF photodiodes are located in pupil planes, thereby avoiding a conversion of wavefront tilting to beam walking on the photodiodes. This is a prerequisite for high quality differential wavefront sensing, which is applied to determine the tilt of the incoming wavefront and the proof mass with respect to the optical bench at nanorad resolution.

The transmit power entering the telescope is about 2 W, while the total received power is only on the order of 200 pW. Therefore, stray light is of severe relevance and must be controlled carefully. One stray-light rejection method is provided by combining the signals from 2 detectors. Such method would also counter the intensity noise. An additional provision for suppression of stray light generated within the telescopes consists of orthogonal linear polarizations between transmit and receive beams as illustrated in Figure 5.2-13. This will be accomplished by installing on one of the two optical benches on board each spacecraft, an additional 90° polarization rotator at the telescope interface.

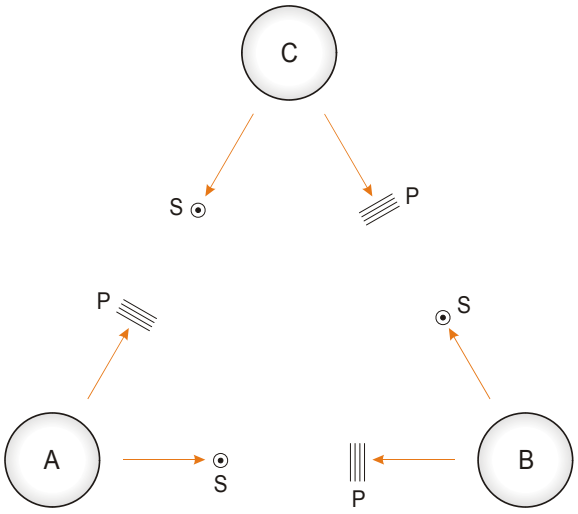

Figure 5.2-13: Send/receive multiplexing scheme. Send and receive beam are separated by using orthogonal linear polarizations on each arm. This leads to three identical spacecraft with two slightly different optical benches.

The Optical Bench contains two different types of mechanism:

- 2 Fiber Switching Units (FSUs)
- 1 Point Ahead Angle Mechanism (PAAM)

The two identical FSUs provide a redundant fiber interface to the second Optical Bench and the associated TX Laser, respectively, and yield a Gaussian laser beam with 2 mm diameter. The PAAM is a single-axis pointing mechanism which sets the in-plane "point ahead angle", i.e. the angle between incoming and transmitted laser beam in the plane of the constellation. The out-of-plane point ahead angle is roughly constant over mission life and has to be set to a static value of 268 µrad on the Optical Bench (before the telescope) by proper alignment of optical components. These mechanisms are described in more detail in paragraph 5.3.8

The Optical Bench will further have to accommodate part of the optics of the telescope, called the "Telescope Back Optics". It consists of the telescope ocular, a "Refocusing Mechanism", and beam routing optics. Therefore, a specific region on the Optical Bench may not be occupied with other equipment.

5.2.1.3 MOSA Sensors

5.2.1.3.1 Quadrant Photo Diodes

The heterodyne signal for the science measurement as well as for the optical readout of the proof mass position and attitude will be obtained from quadrant photodiodes by means of differential wavefront sensing. The required detector properties are driven by the Doppler shift (order of 20 MHz) and the related detector and laser intensity and/or frequency noise figures. As baseline a 0.5 mm diameter quadrant photo diodes made from InGaAs with an integrated transimpedance amplifier is assumed. Figure 5.2-14 shows an example of an Opto-hybrid quadrant photodiode for free space laser communication between satellites,

consisting of quadrant detector chip (frontside) and 4-channel transimpedance amplifier (backside of ceramic substrate).

Figure 5.2-14: As example for a LNA opto-hyrbid set-up with InGaAs QD

5.2.1.3.2 Acquisition Sensor

Initial acquisition of the incoming laser beams from the remote s/c is accomplished with the help of a CCD image sensor on the optical bench, which is used to infer the relative pointing of the s/c in the beginning. It has to provide a sufficient field of view to accommodate the initial pointing error, as well as a resolution compatible with the field of view of the science quadrant photodiode, which will take over for final fine positioning.

In the near infrared range, InGaAs is a mature material offering superior quantum efficiency. Trading of the alternative CCD concepts should respect the actual availability of according sensors. A possible reference architecture produced by FLIR Systems Inc. is shown in Figure 5.2-15. Its main specifications are:

- Resolution: 640 x 512 pixels, 25 µm pixel pitch
- Spectral range: 0.9 – 1.7 µm
- Average quantum efficiency: ~ 65%
- Noise-equivalent intensity (NEI): 0.4 nW/cm^2 @ 16 ms integration time
- Max. frame rate: 107 Hz with 4 outputs
- Power dissipation: < 250 mW
- Operational temperature range: 20°C – 71°C
- Shock, vibration, altitude, and radiation tested

Given the cited NEI, the acquisition beam has to be focused on an area less than 1 mm^2 to achieve an acceptable SNR, a value that should be easily achievable with appropriate imaging optics. It corresponds to an array of 40 x 40 pixels, much more than the foreseen 2 x 2 pixels, the minimum required for the image centroid computation with sub-pixel resolution.

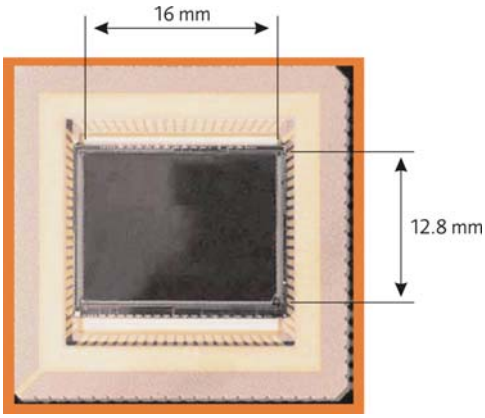

Figure 5.2-15: Large format InGaAs Focal Plane Array (FPA) by FLIR Systems Inc.

5.3 Gravity Reference Sensor System

The Gravity Reference Sensor (GRS) System consists of a GRS Head and the associated GRS Electronics. The sensor head contains the Proof Mass (PM) that acts as the reference point in the LISA interferometric system. The PM is surrounded by an electrode housing (EH) and two caging mechanisms on top and bottom (CMA) that block the PM in a safe position to sustain launch loads and carries it back to centre of the EH where it is released in order to start science operations. The PM, the EH and the CMA are maintained in a high-vacuum controlled environment by means of a dedicated GRS Vacuum Enclosure (VE). Compensation masses are placed in order to create a symmetrical gravitational field in proximity of the Proof Mass. The Charge Management Device (CMD) perform electrical discharge of the PM when required. As mechanical contact to the PM is not permitted, the CMD discharges the Test Mass by shining UV light to selected surfaces both on the PM and on the EH. Figure 5.3-1 shows the block diagram of the GRS

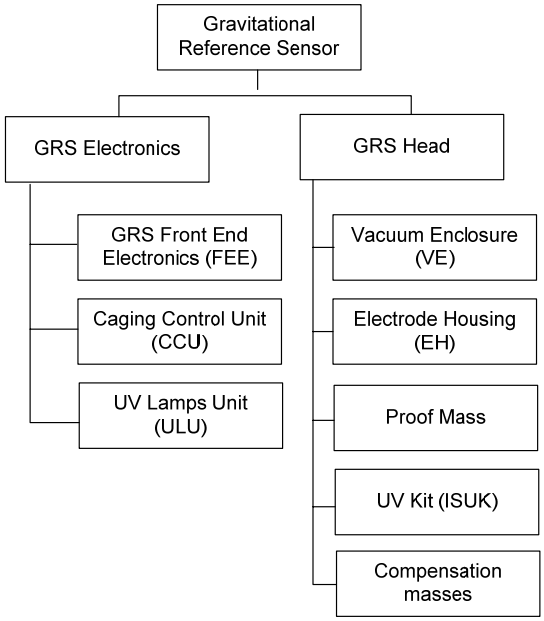

Figure 5.3-1: Breakdown of the GRS System

In nominal science operations, the PM must be kept free-flying, meaning that within the limit of the residual acceleration requirement no forces other than gravity should act on it along the sensitive axis (i.e. the interferometer axis, x). The PM position in the x-axis and the tip and tilt with respect to the sensitive axis are read by the local interferometer. The micro-propulsion system is commanded in order to move the SC and maintain the PM at the centre of the EH. Tip and tilt rotations are instead controlled through electrostatic actuation. The PM control along the non sensitive axes is performed by the electrostatic means for both the read-out and actuation.

Electrostatic read-out is based on the fact that the relative motion of the PM with respect to the EH induces a variation of the gaps between the EH and PM and therefore of the relevant capacitance. This is used to detect the TM motion via a set of parametric-bridge based, differential capacimeters. The GRS Front End Electronics (FEE) provides the readout of the capacitive sensing and also applies the requested voltages to the EH electrodes for TM actuation.

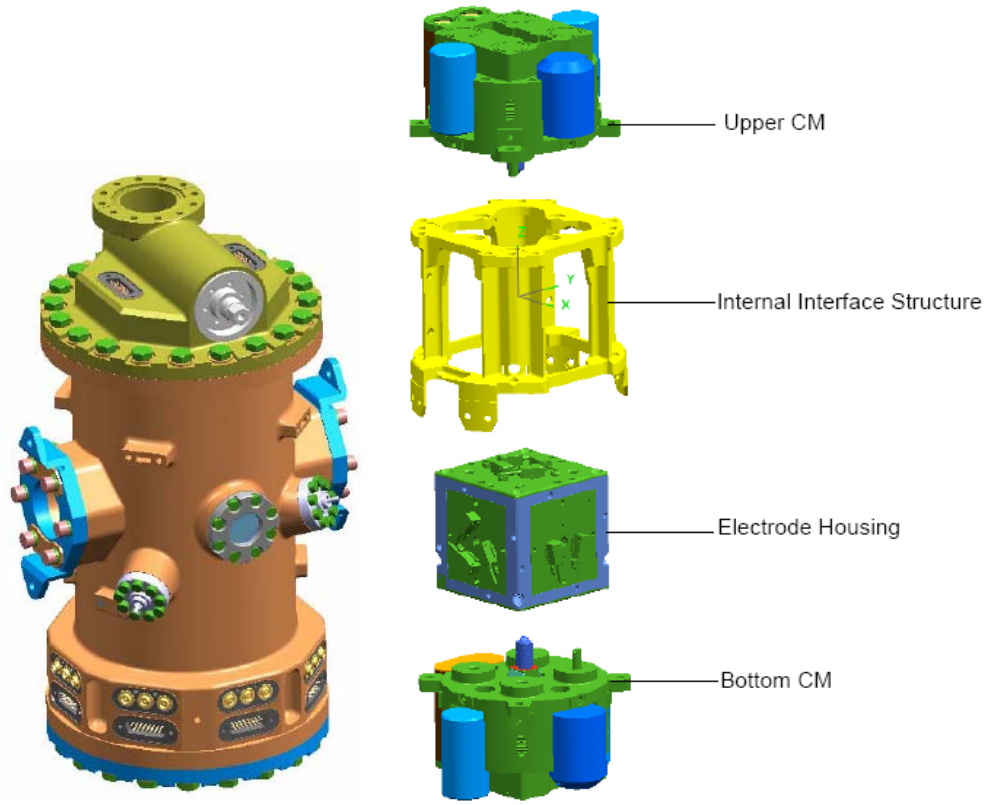

Figure 5.3-2: Inertial sensor assembly.

5.3.1 Proof Mass

The proof mass is a cube made of Gold-Platinum with an edge-length of 46 mm. The chosen material has a very small magnetic susceptibility making it less sensitive to the magnetically induced disturbance accelerations. . The pyramidal recess is centered on the +/-Z cube faces. Cube corners are rounded with offcentered spherical cuts. Figure 5.3-3 shows an engineering model of the proof-mass.

Figure 5.3-3: Proof Mass (EM).

5.3.2 Electrostatic Actuation and Readout

The electrostatic actuation and readout is performed by the Sensing and Actuation Unit (SAU), part of the GRS FEE. The SAU consists of two sets of six perfectly balanced, displacement-sensing channels and two sets of twelve actuating channels, with associated transformers, analog-to-digital converters (ADC), digital-to-analog converters (DAC), chains of extremely low-noise amplifiers, modulator and demodulators. The digital control logic and high-speed communication with the control computer is handled by an application-specific digital logic enclosed with the analog electronics.

In the framework of LISA Pathfinder, a detailed trade-off for the best electrode configuration has been done. The result is the electrode configuration presented in Figure 5.3-4, and the same configuration will be used for LISA. The green electrodes are used to inject a high-frequency signal to the PM. The yellow electrodes are the actuation electrodes in the sensitive axis. The red electrodes are the actuation electrodes in the non-sensitive axes. Note that the injection electrodes in the z-axis are split into two smaller sets due to the large hole for the plungers of the caging mechanism.

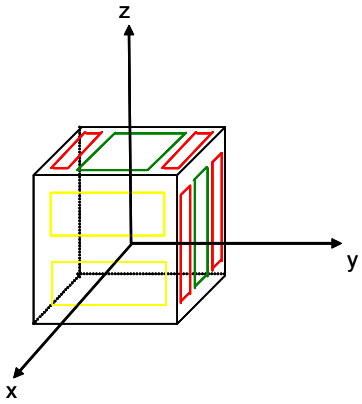

Figure 5.3-4: LISA Pathfinder LTP electrode configuration.

The principle for providing an electrostatic readout is based on a standard resonant bridge scheme where the capacitance modulation of two opposing electrodes due to the test-mass motion is detected as an imbalance of the bridge. The circuitry is illustrated in Figure 5.3-5.

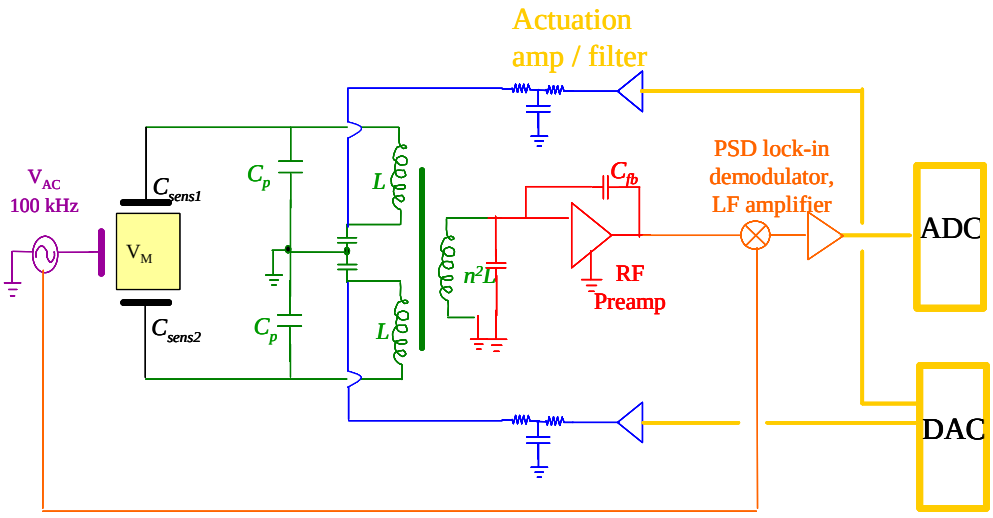

Figure 5.3-5: Sensing and actuation circuitry.

The GRS Front-End Electronics includes all electronics devoted to the test mass position and attitude control, displacement and attitude measurement, biasing and dithering, power supply and basic acquisition, but excluding data processing and experiment management and control (DFACS)

5.3.3 Electrode Housing

Figure 5.3-6 illustrates the electrode housing assembly including all electrodes as well as the corresponding engineering model of LPF (equipped with thermistors for testing). The housing is made of Molybdenum, while the electrodes (yellow) are made of sapphire. Most surfaces are gold plated.

The EH surrounds the six TM faces. It is composed by the molybdenum Support Frame (SF) holding the six Support Plates (SP) on which the electrodes are mounted.

The eighteen electrodes (four X sensing, four Y sensing, two Y injection, four Z sensing, four Z injection) are characterized by five different dimensions types. All electrodes and EH parts surfaces facing the TM are gold plated. The electrodes are surrounded by edge guard rings extending into the "shadow" of the capacitive sensor by a distance equal to that of the gap width on the given face of the sensor.

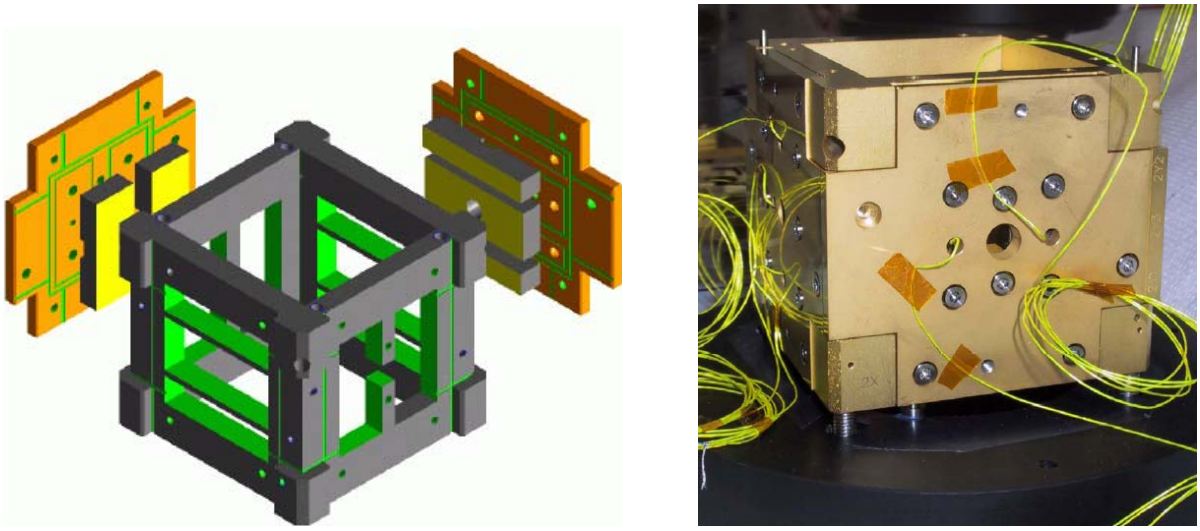

Figure 5.3-6: Electrode Housing Assembly and EM.

5.3.4 Caging Mechanism

The caging mechanism is powered via the Caging Control Unit (CCU) and will be actuated in order to ensure the PM integrity during launch and to release it before the science operations begin.

Each CM is done divided in 2 actuators, (+Z Caging Mechanism and Actuator Unit and –Z Caging Mechanism and Actuator Unit). Each actuator is divided in 2 main sub-mechanism:

- The Grabbing, Positioning and Release Mechanism (GPRM)
- The proper Caging Mechanism (CMSS).

These 2 sub-mechanism perform different functions. The Caging SubSystem Mechanism (CMSS) uses four fingers to press the PM against dedicated stops in order to perform the high and medium load functions required for holding the PM during launch and storage. The GPRM instead is mainly responsible for performing the low load functions. Notably it uses a cascade of two concentric fingers to position the PM at the centre of the EH and to perform the final break of the adhesion forces between the PM and CMSS fingers allowing the hand over to the electrostatic control of the PM.

The CCU will be fully commanding both the CMSS and the GPRM and will give information about the mechanisms actuators and load feedback to the higher level control authority which will coordinate the actions with the other subsystems (notably the GRS FEE during the phase of PM release) to perform the functions requiring coordination

5.3.5 Charge management system

LISA Charge Management Device (CMD) system is largely based on that of LPF. The PM is discharged using UV light via the photoelectric effect. Depending on the polarity of the PM charge, the surface of the PM itself or those of the EH will be used to release photoelectrons.

The UV light is transmitted from the ULU (UV Lamp Unit) where it is produced, via the FOH (Fiber Optical Harness), to the GRS Vacuum Enclosure. There, through the ISUK (Inertial Sensor Ultraviolet Kit), comprising Ultra High Vacuum feedthrough is transmitted to the inside to the Electrode Housing. Each GRS has three UV feedthroughs embedded in the VE. Each feedthrough is connected to one lamp. The baseline CMD design is such that each feedthrough nominally has the same range of UV photon output. In each sensor, two feedthroughs point towards the EH and one points towards the TM. To discharge a positively charged TM, the feedthroughs pointed towards the EH will be used. To discharge a negatively charged TM, the feedthrough pointed towards the TM will be used.

5.3.6 Self Gravity Compensation

The gravitational effect of the payload and spacecraft on the two free-floating proof-masses must be compensated. This reduces the DC forces and torques on the proof-masses which have to be compensated either by the Drag Free Control System or by the electrostatic actuation

In addition to the DC forces, the first derivatives of the gravitational effects must be made small. This so-called self-gravity stiffness induces an inherent instability to the dynamics of the proof-masses which also drives the required bandwidth of the electrostatic suspension controllers in the non-sensitive axes. A higher bandwidth also drives the required voltages of the suspension control system and increases the disturbance accelerations due to cross-coupling effects into the sensitive axis.

The spacecraft design has already been also analyzed and boxes are arranged such that the self-gravity effects on the two proof-masses are minimized. For compensation of residual effects, locations for compensation masses are foreseen first inside and then very close to the GRS assembly. The required distribution of compensation masses can only be obtained on the basis of a gravitational analysis of the final FM spacecraft and payload design, very late in the implementation phase.

As an example in LISA Pathfinder, the material used for the balance masses is the alloy Tungsten 90% Copper 10%. This alloy has a mass density of 16900 kg/m3 and the internal balance masses weight is about 1.8kg. The balance masses are mounted to fill the reserved available room between the IS and the Vacuum Enclosure. The maximum masses that can be accommodated within the available volume are shown in the following picture

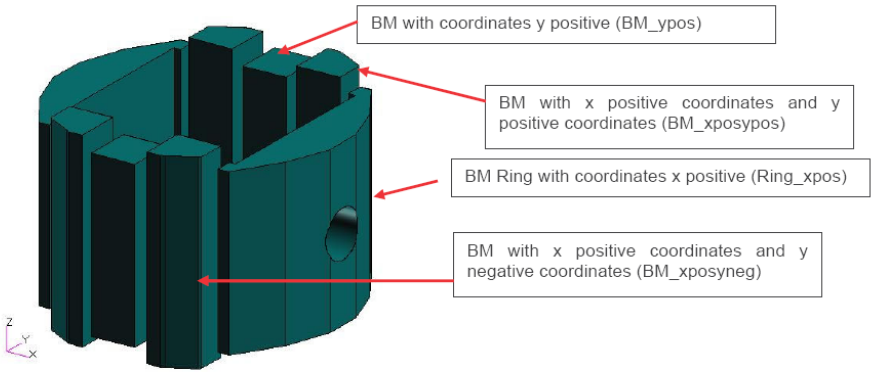

Figure 5.3-7: Compensation masses.

5.3.7 GRS Functional Architecture

The functional interaction of the components described above and of required drive electronics can be summarised in a functional architecture as shown in Figure 5.3-8. The electronics attached to the GRS head are Front-End Electronics (FEE), UV Light Unit (ULU) and Caging Control Unit (CCU).

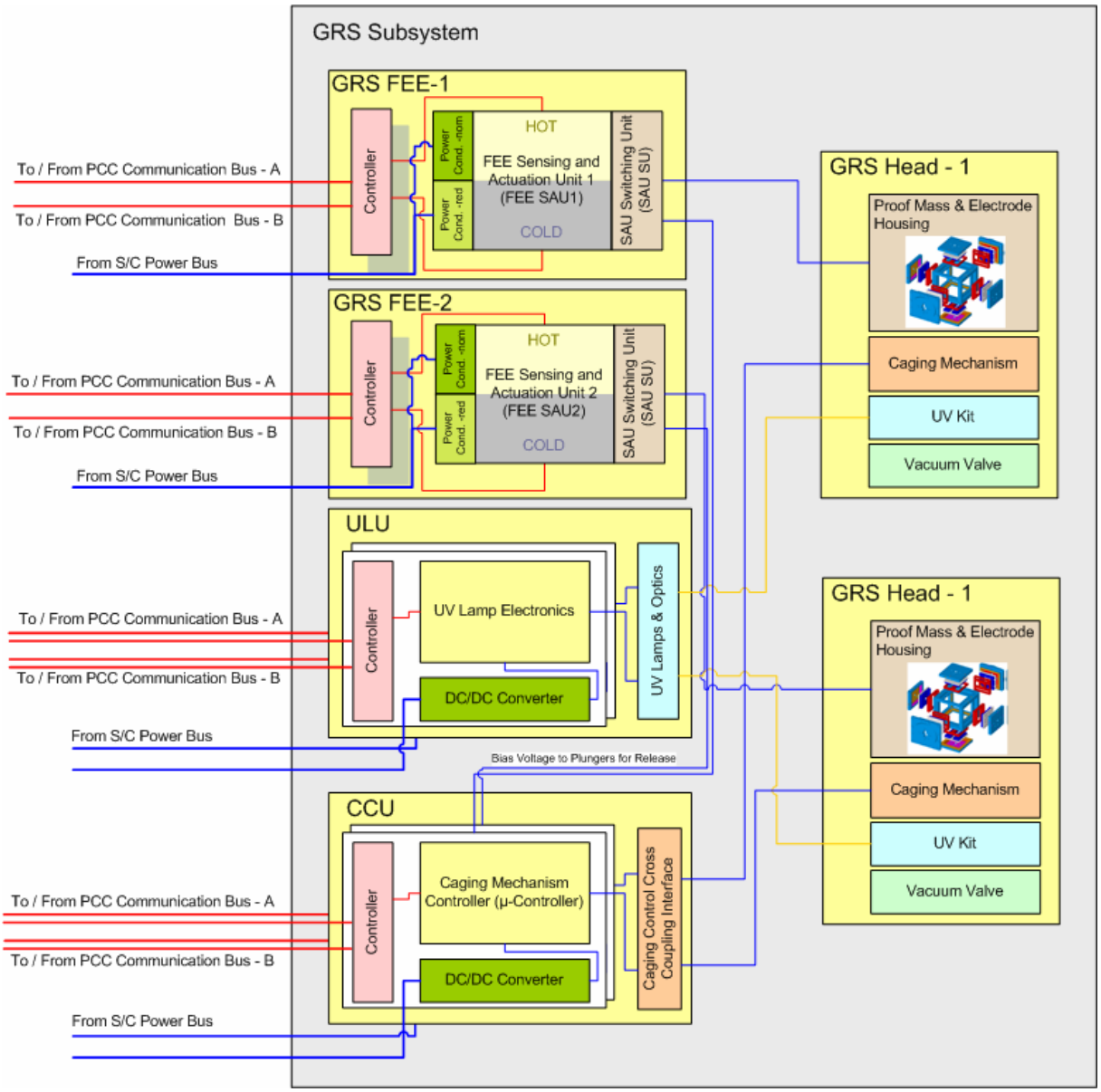

Figure 5.3-8: *GRS Functional Breakdown and Interlinks*

5.3.8 Payload Mechanisms

5.3.8.1 Optical Assembly Tracking Mechanism

The pointing of the two telescopes for correction of the seasonal LOS angle variation will be realized by combining a single-axis mechanism controlling the angle between the telescopes with the micropropulsion thrusters controlling the attitude of the entire spacecraft. For LISA, the proposed telescope pointing architecture is:

- Use of the spacecraft attitude control to realize a complete pointing of one MOSA and of the off-plane angle of the second telescope (of the other MOSA)
- Use of a mechanism to control the in-plane angle of one MOSA
- Implement a spare mechanism, so that the roles of both MOSA can be switched in case of failure.

Therefore, each MOSA is independently supported and equipped with a single axis mechanism. The overall operational range of about ± 1.5° around the mean position, results from the requirement that each MOSA shall be able to cover the complete excursion range.

The required MOSA movement will be performed by the Optical Assembly Tracking Mechanism (OATM) which is an assembly of actuators, flexible pivots, launch locks and the MOSA harness.

The OATM is used as part of the actuator system of DFACS. All driver electronics for the OATM components will be housed in the OAME.

One main driver for the selection of the OATM components is the torque noise requirement, which is derived from DFACS analysis. This requirement is broken down to the OATM components - the values can be seen in Figure 5.3-9. Most of the already very low torque noise budget was allocated to the actuator as this active component is seen as the major contributor to torque noise in the system.

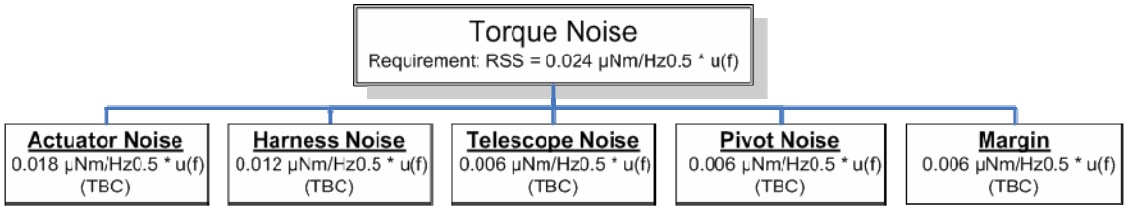

Figure 5.3-9: *Breakdown of Torque Noise Requirement for OATM*

The small required rotation angle, the high motion resolution and the requirement for low induced noise leads to the use of flexible pivots as a preferred telescope bearing system baseline. Such spring elements provide sufficient load carrying characteristics to support the operational loads during on ground test, launch and on orbit. The mechanical layout for the optical assembly actuator and pivot system is arranged such that the rotation axis of the optical assembly ideally runs through the centre of mass of the individual MOSA. This means an off-set arrangement of the PM, but self-gravity analyses have demonstrated this not to be a problem. Therefore, the static unbalance of the MOSA is very small and so reduces loads on flex pivots and launch lock device.

Two different concepts are viable for the design of the OATM: a combination of a coarse pointer for the achievement of the long range position with a superimposed fine pointer for tuning the final end position, or a single stage solution using a high resolution tracking actuator.

As baseline, the NEXLINE® actuator concept is chosen, whose principle is that of a linear piezo motor. Non-resonant piezo motors usually consist of several individual piezo actuators and generate motion through succession of coordinated clamp/ unclamp and expand/contract cycles. Each extension cycle provides only a few microns of movement, but running at hundreds of Hertz, achieves continuous motion in the mm/second range. The latest NEXLINE® piezomotor designs address the drawbacks of existing nanopositioning drives. NEXLINE® systems are based on very rugged, high-efficiency shear actuators and incorporate a preloading mechanism to provide pushing and holding forces up to 600 N with basically unlimited lifetime. Such motors combine two operating modes: in long-range step mode, motion consists of user-defined (or auto-ranging) steps with widths from less than 1 nm to 6 µm in size; in fine-adjustment mode analogue piezo motion with subnanometer resolution over a travel range up to 6 µm is provided. For the LISA Payload, a hybrid concept is proposed which combines stepping and analogue mode such that very high travel ranges and a noise reduced motion can be achieved. This requires adequate adoption of the driver electronics and will be optimised to meet the required performance.

The design concept of a linear piezo motor increases the flexibility of the envelope location. For the current OATM design, the actuator is attached to the conical end of each MOSA. Supported by the middle beam of the OAM framework, the actuators will be mounted near to the launch lock device (see Figure 5.3-10). By this design a long lever can be provided which enhances the angular resolution of the OATM and structural rigidness is improved as the actuator and LLD will transmit centrally loads to the MOSA.

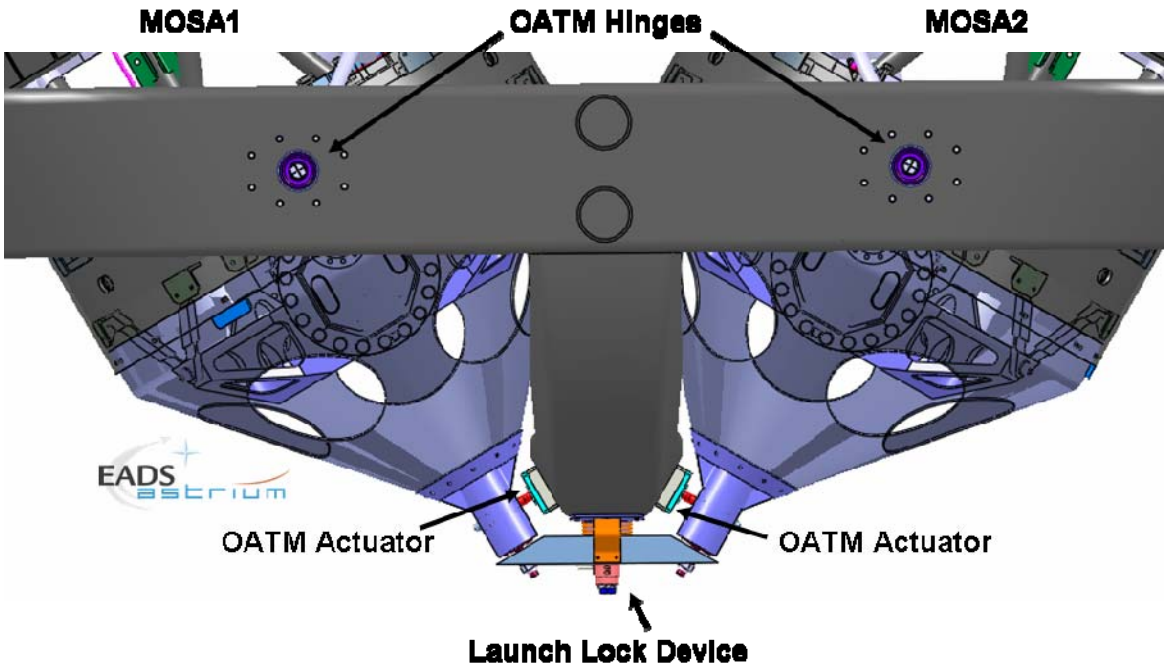

Figure 5.3-10: Locations for the NEXLINE® tracking mechanism.

The current design performance of the OATM Actuator can be seen in Table 5.3-1. This assumes a dedicated structural design (wrt. lever arms) and the hybrid motion case for an Inchworm actuator. As can be see in the table, the angular resolution will be determined by the digital to analogue converter DAC which will provide high voltage supply to the piezo driven actuator. Preliminary analyses have shown that this performance is in line with the DFACS acquisition and science modes. Further improvements in pointing accuracy are the augmentation of DAC resolution and sampling frequency which will then become a design driver for the OAME

OATM design fact sheet	Value	Annotation
Actuator max analogue Movement / µm:	3	Actuator and Controller Properties
Voltage range / V:	250	
DAC - resolution / bit:	12	
Sampling Rate / Hz:	10	
Displacement Error due to Quantisation / nm:	0.732	Performance for Acquisition
Angular Error due to Quantisation / nrad:	2.154	
Displacement Noise due to Quantisation / nm/√Hz:	0.134	Performance for Science Mode
Angular Noise due to Quantisation & Sampling / nrad/√Hz	0.393	

Table 5.3-1: *Angular Resolution and Noise due to Actuator Command Quantisation, Values for an Inchworm Actuator*

For initial pointing acquisition, the pointing mechanism can be fitted with an internal sensor capable of delivering absolute knowledge about the actual pointing. Once the acquisition is completed, precision sensing of the instrument pointing will be provided by differential wavefront sensing on the science photodiodes, which will then be used for closed loop control of the OATM by DFACS.

5.3.8.2 Point Ahead Angle Actuator

The “Point Ahead Angle Mechanism” (PAA) is a mechanism adjusting the wavefront tilt of the received science beam before interference with the local oscillator beam on the science detectors. This adjustment is required to compensate for the seasonal change of the angle between received and transmitted laser beam of each telescope assembly, called the point ahead angle. It results from the orbital motion of the three spacecraft with respect to each other and the 16 s travel time of the laser light between the spacecraft.

As discussed in above, only the out-of-plane component of the point-ahead angle requires correction, so that a single-axis mechanism is sufficient. It will be located on the optical bench in a pupil plane of the telescope, in order to provide pure angular correction. As part of the science chain, the PAA mechanism has to respect extremely stringent requirements, which are summarized in Table 5.3-2.

Quantity	Requirement	Comments
Full pointing range	±350 µrad	Accommodate out-of-plane point-ahead variation of ±6 µrad, including telescope magnification of 80, initial misalignment of ±50 µrad, and 20% margin.
Absolute pointing knowledge	±4 µrad	Ensure an external pointing error of less than ±0.1 µrad.
Maximum pointing jitter	$15\,\frac{\text{nrad}}{\sqrt{\text{Hz}}}\times\sqrt{1+\left(\frac{2.8\ \text{mHz}}{f}\right)^4}$	Achieve same jitter performance as provided by proof-mass optical readout in rotational angles.
Maximum fine pointing rate	70 prad/s	Maximum rate for sine motion with 700 µrad peak-peak amplitude and 1 year period.
Maximum coarse scan rate	100 µrad/s	Obtain reference position in less than 10 s.
Overall piston error	$3\,\frac{\text{pm}}{\sqrt{\text{Hz}}}\times\sqrt{1+\left(\frac{2.8\ \text{mHz}}{f}\right)^4}$	

Table 5.3-2: Preliminary performance requirements for the point-ahead angle mechanism. Note that angular requirements correspond to the mirror tilt angle, which is half the beam deflection angle. All values are TBC.

An advanced design concept for the PAA mechanism is illustrated in Figure 5.3-11. It is based on a Gimbal actuation principle, which inherently avoids piston effects due to tilting. The complete structure is monolithic, with integrated elastic Haberland hinges, and made from a stable material, e.g. TiAlV. The actuator is a piezo stack providing high resolution and sufficient stroke. It is integrated in redundancy to a second piezo via a common lever. The lever arm between the piezos and the mirror is tunable and thus optimizable for best performance. No launch lock is required.

A passive thermal compensation accounts for the thermal expansion mismatch between piezo and housing. In combination with the symmetric design, thermal expansion can thus be kept sufficiently low to limit the associated mirror piston motion to within the requirement. The forces on the mirror are arranged to be parallel to the mirror plane, which prevents distortion of the mirror surface.

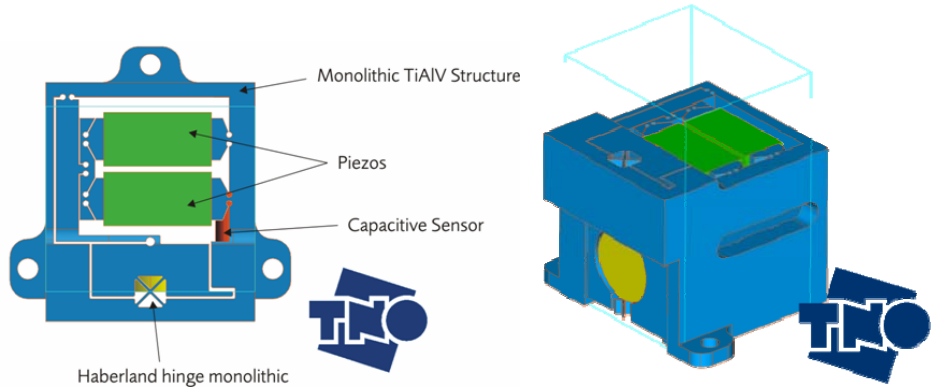

Figure 5.3-11: PAA mechanism conceptual design.

An integrated position sensor (e.g. a capacitive sensor) provides information on the actual mirror tilt angle. In a closed loop control, the piezo drift and hysteresis can be minimized and the mirror pointing with respect to the optical bench can thus be acquired with sufficient accuracy. The resolution of the position sensor is

sufficient to enable control of the mirror pointing jitter, despite angle disturbances due to DAC quantization noise, piezo amplifier noise, piezo motion creep and limited sensor resolution itself.

The design allows for a full pointing range of ±500 µrad, corresponding to a piezo stroke of ±10 µm. From a preliminary noise assessment, an absolute pointing knowledge of 3 µrad and a pointing jitter of approx. 12 nrad/√Hz is expected, in compliance with the requirements. To achieve this performance, the mechanism has to rely on a maximum voltage noise spectral density of at least 1 mV/√Hz and the high thermal stability in the optical bench environment (10^{-5} K/√Hz). The jitter of piezo position due to temperature fluctuations is however expected to be negligible.

Due to the low bandwidth actuation of the PAA mechanism, the expected heat dissipation to the optical bench should be negligible. A maximum dissipation of about 10 µW is expected in nominal operation, corresponding to residual electrical losses for quasi-DC operation.

5.3.8.3 Fiber Switching Unit

Purpose of the Fiber Switching Unit is to provide a switching capability for selection between redundant laser systems, as well as a possible fine adjustment of the beam pointing at the fiber launcher position on the optical benches. The concept of the baseline FSU bases on a rotatable waveplate which performs the actual switching capability. This concept is depicted in Figure 5.2-31 below.

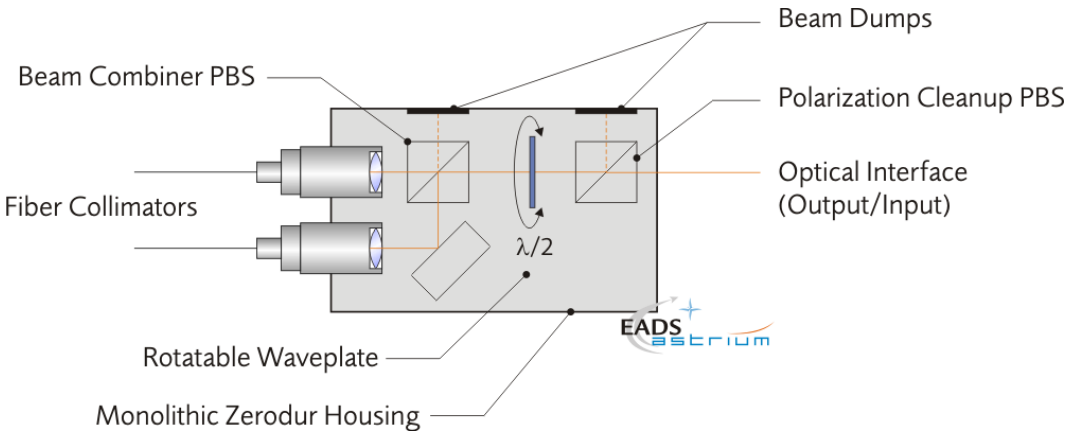

Figure 5.3-12: Fiber positioning unit - type fiber translation

By this design, a cold redundancy of two alternative laser systems can be achieved per OB and for the backside fiber. It provides an optimum alignment stability as lifetime effects change only optical performance but no mechanical re-positioning of the optical components themselves. These components will be bonded onto a monolithic ZERODUR housing.

5.3.8.4 Launch Locks

As the performance requirements of the OATM, especially the torque noise requirements, require the use of torsion-soft flexural pivots, the launch loads onto the OATM cannot be withstand by the flex pivot. Therefore, a dedicated component is under development which will house the flex pivot but also will provide an

alternative, rigid and stiff load path for the launch configuration. This component will be actuated once with a launch lock device (LLD) typically as described below. With this LLD actuation, the nominal load path will be freed such that the flexural pivots will be the single, rotational support of the MOSA to the OAM frame structure.

The second type of LLD is the one at the very end of each MOSA (see Figure 5.3-10). This suppresses in launch configuration the movement of the MOSA around its pivot axis. The second main task of this device is to minimize loads onto the OATM actuator such that its holding forces will not be exceeded. Beyond holding forces and in off-mode, the OATM actuator is holding the rod's position only by friction forces, thus the rod must not move as the surfaces of this device could be damaged by scratching.

A typical LLD design can be seen in see Figure 5.3-13. The separation happens between cup and cone after releasing the preloaded HDRM-bolt which is retracted into the bolt catcher. The cup and cone system is able to transfer bending moments as well if preloaded with adequate force. Such a pyro-less device is proposed to be used for the release mechanism of the MOSA.

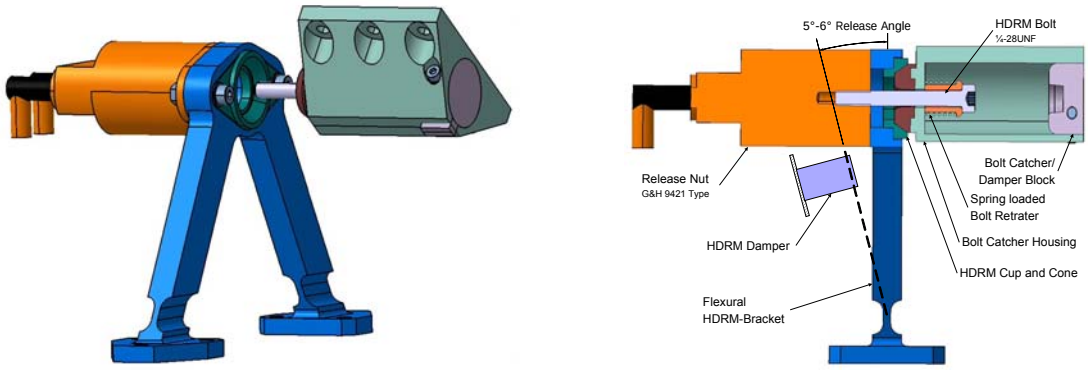

Figure 5.3-13: HDRM example with corresponding section on right.

For release of the preloaded HDRM-bolt, G&H Technology, Inc. has developed a solution to separate structural items without application of pyrotechnic devices. It offers fast and gentle low shock separation and is fully re-settable. The principle of operation is illustrated in Figure 5.3-14. The operation of the separation nut starts with the spool-release initiated by a standard spacecraft electrical pulse breaking a fuse wire holding the spool in place.

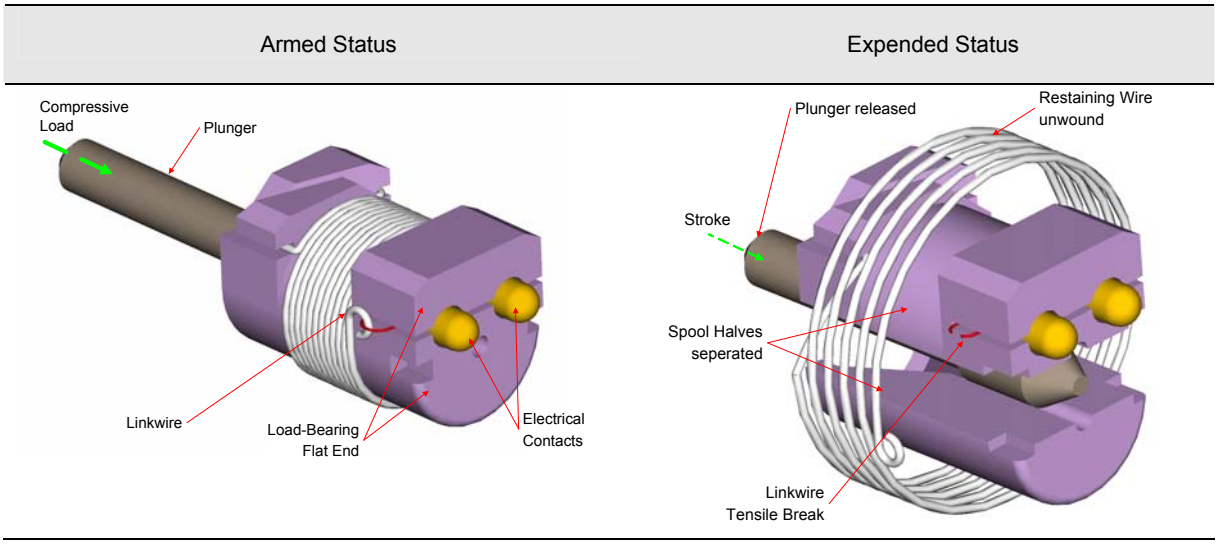

Figure 5.3-14: G&H spool-initiated device principle.

The separation nut is implemented in redundancy to a second release spool device in the actual release mechanism, which is illustrated in Figure 5.3-15. The action of either one of the two redundant spools leads to the movement of the central point of a common lever, over which they are combined. This movement liberates the associated degree of freedom of a larger preloaded cylinder, which thereby removes blockages of another mechanism that finally releases the HDRM-bolt.

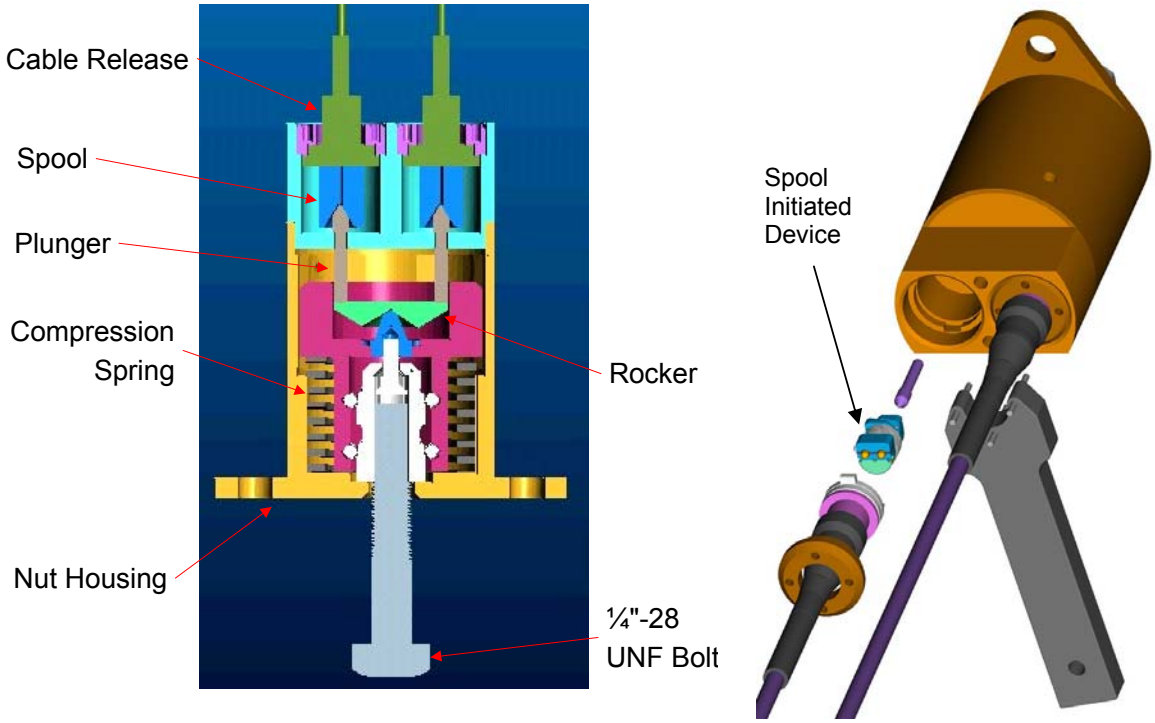

Figure 5.3-15: Section of the release mechanism.

5.4 Phase Measurement Subsystem

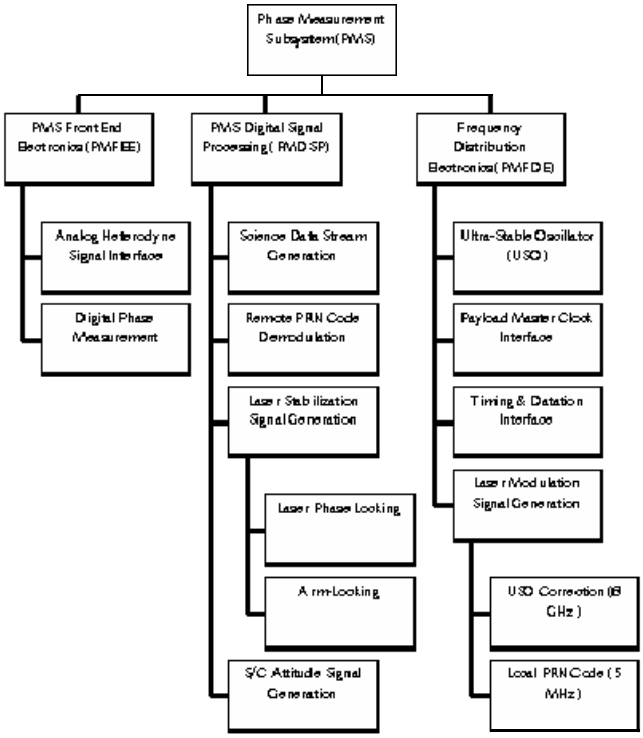

Figure 5.4-1: *Breakdown of the Phasemeter Subsystem*

The Phase Measurement Subsystem (PMS) consists of the Frequency Distribution Electronic (PMFDE) providing the frequency reference (Ultra Stable Oscillator, USO) for the measurement and the phase meters and an associated digital signal processor (PMDSP). Apart from performing phase measurements on the interferometer signals, the PMS post processes the raw measurements as needed for the science data stream and the on-board uses. As ancillary functions on board time keeping for the science measurements, management of the inter-spacecraft (optical) data link, inter spacecraft exchange of time semaphores and controlling of laser frequencies are performed by the PMS.

5.4.1 General Functions

The PMS performs the phase measurements on the beat signals of the optical interferometers used in the payload of the LISA spacecraft. It measures the phase of sinusoidal signals relative to an internal time reference (USO) with high precision (about 10^{-5} rad /√Hz), The measurements are processed by the PMS as needed to serve three different purposes

- Provide phase measurements the science data stream. For this purpose the raw measurements are decimation-filtered to represent a 1 Hz bandwidth low pass signal samples at 3.3 Hz, encoded, annotated with time stamps and packetized.
- Provide angular measurements for use in the drag free attitude control system. For this purpose selected phase measurements are processed to represent differential wavefront sensing signals at 5 Hz B/W (10 Hz sampling) with real time bandwidth as needed for the attitude control function
- Provide frequency measurements as to be used as sensor signal for the laser frequency control. For this purpose selected measurements are processed to represent frequency measurements with a bandwidth of about 50 KHz and real time properties as needed for the purpose of laser frequency control

In conjunction with these main functions ancillary functions are performed by the PMS which are due to technical constraints best performed in conjunction to the phase measurement task:

- Implementation of a frequency reference for the spacecraft science measurements (USO)
- Generation of RF modulation tone for USO phase noise measurement (a signal at about 10 GHz synchronously derived from the USO to be phase modulates onto optical intra-spacecraft link)
- Implementation of time stamp for internally generated data and the DFACS synchronisation signal
- Demodulation of data modulated onto optical inter spacecraft links
- Provision of encoded modulation signal for local lasers (both laser signals generated on a LISA spacecraft are phase modulated with a single tone RF signal for USO frequency noise measurement and a (baseband) direct sequence PN encoded data modulation)
- Management of time-stamp exchange and routing of data communication
- Implementation of controllers for laser frequency control loops (two on each space craft)

5.4.2 Phase Meter Functional Breakdown

The phase measurement subsystem consists of the frequency distribution electronic providing the frequency reference for the measurement (USO) and the phase meters and an associated digital signal processor.

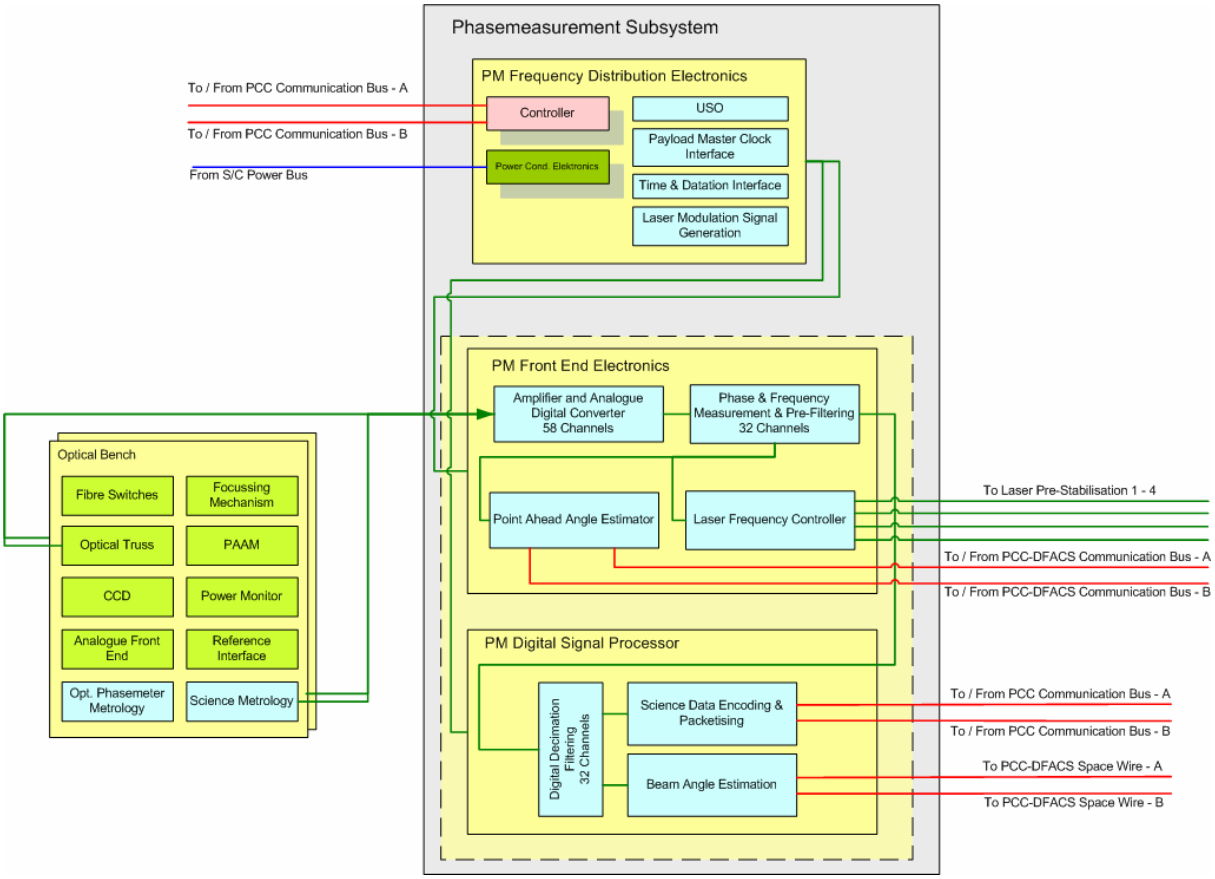

Figure 5.4-2: *Phase Measurement System Functional Breakdown*

The PMS units and its functions are:

- Phase Measurement Frequency Distribution Electronics (PMFDE)
  This unit contains an ultra stable oscillator (USO; about 10^{-12} Allan standard deviation) and frequency converters as neded to generate the RF modulation signals the reference clock of the phase meter electronics and the phase meter pilot tone.
- Phase Measurement Front End Electronics and Phase Meter Digital Signal Processor (PMFEE and PMDSP)
  It is presently assumed that the complete functionality is included in a single housing. The PMFEE/PMDSP processes the detector signals which are provided to it via dedicated analog interfaces, a separate interface for each quadrant of every detector. The PMFEE/PMDSP performs following functions on the signals:
  - select redundancy
  - combine input signals as input to phase measurement (a measurement can be performed on the sum of 1 up to 4 different inputs or the difference of two of those sums)

- perform measurements on the input linear combinations (the measurements can be either a phase measurement on a main beat note, a differential phase measurement on two modulation sidebands, a frequency measurement on a main beat note or differential phase measurements on two main beat notes of two different signals).
- low pass filter the raw measurements as needed for the different applications within the LISA system (science data are filtered to 1 Hz bandwidth with no delay time requirement whereas measurements to be used for on board control loops are filtered to higher bandwidth with maximum delay time requirements being applicable)
- encode science data streams and generate data packages annotated with on-board time (actually the on-board time maintained by the PMS as opposed to the time system maintained by the OBC for the purpose of mission control)
- implement the laser frequency control loops, using frequency measurements as sensor information and the lasers as actuator (dedicated interfaces between the frequency control inputs of the lasers and the PMFEE/PMDSP are provided)
- implement a datation system allowing to reference all PMS measurements to on-board time (the latter is given by a counter synchronised to the USO frequency); the datation system also is used to determine the relation of the DFACS reference clock to the on-board time
- perform de-modulation of the direct sequence PN-code modulation on the received inter spacecraft link
- provide a baseband signal for the outgoing data link to be modulated on the respective laser signal
- exchange time semaphore data packages via the inter spacecraft link (which implies measurement and datation of the code phases on incoming and outgoing PN signals)
- implement a data routing function on the inter spacecraft links (used by the OBC as auxiliary communication channel)

Summary of Phasemeter Channels

A summary of the required number of PMS channels is given in Table 5.4-1. It is noted that the 40 active channels simply refer to the number of active lines. PMS internal, only 32 active channels will be processed due to summation of 2 signals of the science interferometers.

	MTR Architecture				MDR Architecture		
Function	Diode Type	Number of Diodes	Number of Analog Chains	Active Channels	Number of Diodes	Number of Analog Chains	Active Channels
Science Interferometer	QPD	2 x 2	16	16	2 x 2	16	16
Reference Interferometer	SEPD	2 x 2	4	2	2 x 2	4	2
Optical Readout	QPD	2 x 2	16	8	2 x 2	16	8
PAAM Metrology	QPD	-	-	-	2 x 2	16	8
Optical Truss	SEPD	-	-	-	2 x 3	6	6
Sum			**36**	**26**		**58**	**40**

Table 5.4-1: Required number of channels of the Phase Measurement System provided by the Optical Assembly

5.5 Laser Subsystem

The laser subsystem contains of 4 independent laser units and a frequency stabilisation unit on each SC. Two lasers provide the light for the transmission to each MOSA in 1 out of 2 cold redundancy scheme. The opto-mechanical switches for the redundancy selection are located on the optical bench.

The present baseline is that the optics and electronics are packaged into a single box for each of the 4 lasers. The laser light is modulated by single tone RF phase modulation (used to measure the Ultra Stable Oscillator frequency noise) and a baseband data modulation (direct sequence PN code). The respective modulators and their electrical drivers are part of the laser units (the modulation signals are provided from the phase measurement subsystem). The lasers can be controlled in frequency via a dedicated interface to the phase measurement system. For at least 5 lasers in the constellation (slaves) the frequency setting results from operating an offset locking control loop with phase meter measurements as sensor input. The controllers are part of the phase measurement subsystem. The remaining (master) laser is controlled by the laser pre-stabilisation subsystem (LPS) to provide a laser signal with sufficient low frequency noise.

The laser pre-stabilization system contains a suitable reference (a cavity in the current baseline) and all necessary electronics needed to stabilise any of the 4 lasers such that its phase noise meets the specified requirements when used as master laser. All optical and electrical switches to select any of the 4 lasers as stabilised master laser are included in the LPS.

A solution has been designed consisting in pre-stabilise the master lasers with respect to a tuneable reference. In such a way a further stabilization loop can be introduced using the interferometer arm as a delay line (arm locking). The cascade of the two pre-stabilization loops further reduces residual laser phase noise impact before the ground post-processing (TDI).

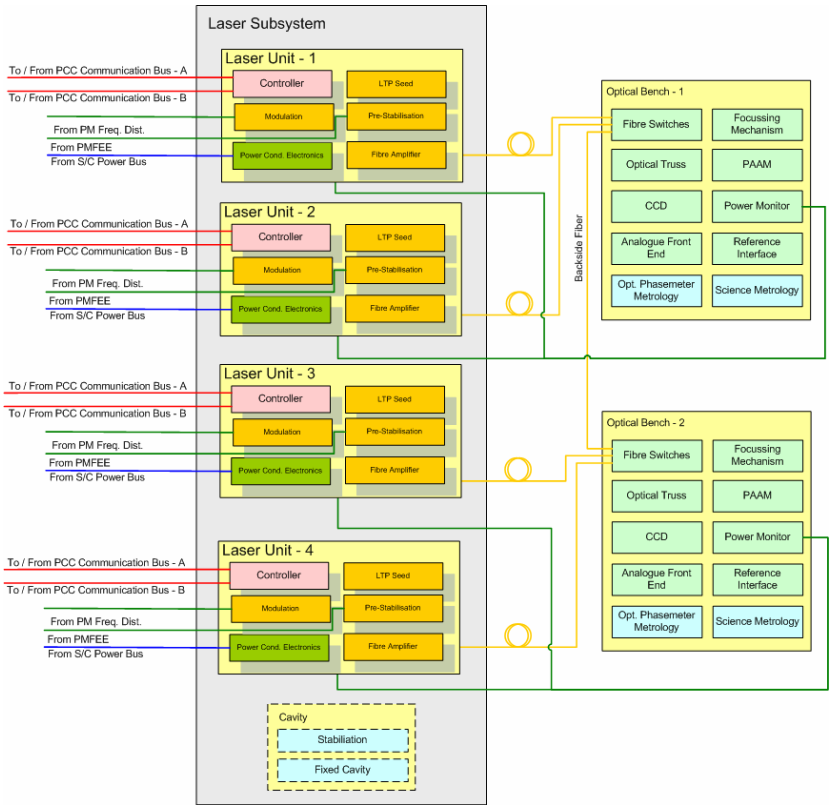

Figure 5.5-1: *Laser Subsystem Functional Breakdown and Interfaces*

5.5.1 Functional Description

A functional architecture for the Laser Subsystem is illustrated in Figure 5.5-2.

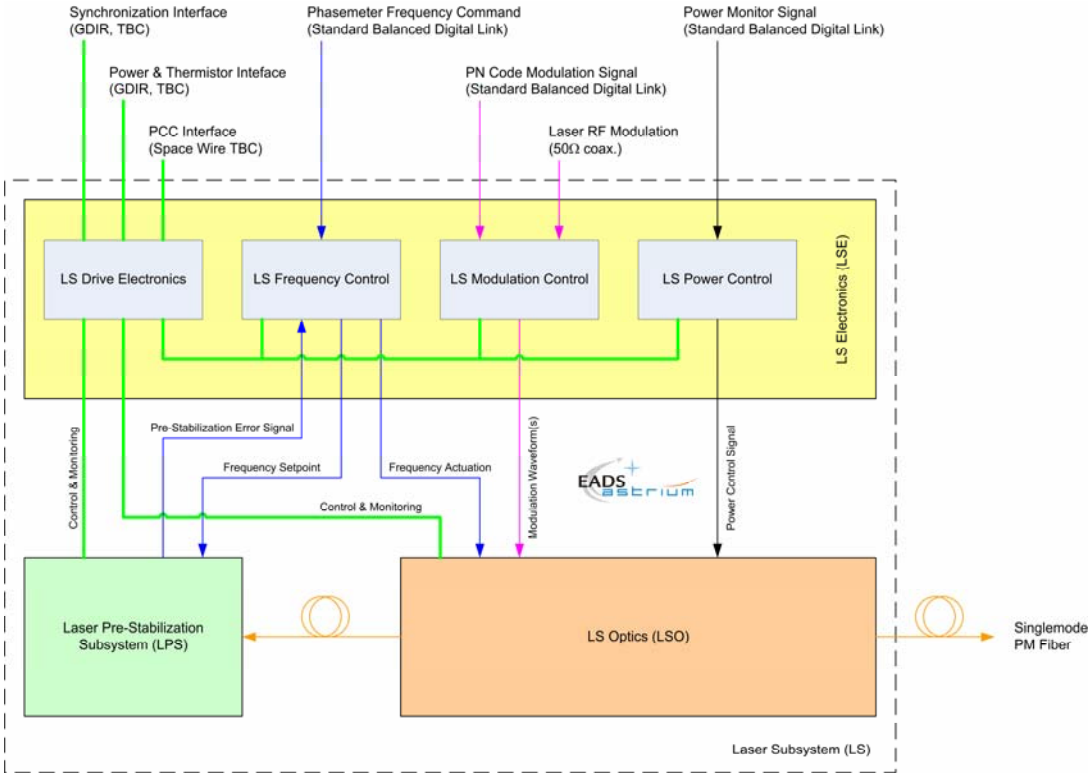

Figure 5.5-2: *Depicted Functional Description of the Laser Subsystem*

The Laser Subsystem has a single optical output in the form of a polarization maintaining single-mode optical fiber with an APC plug. At this output, the LS has to provide a linearly polarized, continuous wave laser beam with a total power of about 2 W end-of-life at a wavelength of 1064 nm. For laser beam spatial acquisition, it must be possible to completely switch off the laser light at this output, without inducing effects that could lead to dead times for switching the laser back on, such as thermal drifts in the system.

The LS has several electrical interfaces for control and monitoring. It interfaces the Control Computer for coarse setting of the laser power and frequency, as well as health monitoring. It interfaces also the Phase Measurement system for the following functions:

- Phase lock for slave lasers, where the laser output is locked (with an offset according to the frequency plan) to the incoming laser beam; or Arm-Locking pre-stabilization where the phasemeter generates a digital error-signal for further frequency stabilization of the Laser Subsystem
- Frequency Modulation: The phasemeter generates two modulation waveforms, which must be applied with appropriate modulation index (amplitude) to the laser light: A PN Code Modulation with a bandwidth of 5 MHz, which is supplied as a digital signal; and a pure sine tone at 8 GHz. For this signal, any excess frequency jitter would have a performance impact and must therefore be avoided. Therefore, this signal shall be transferred onto the laser light as directly as possible. It is supplied via 50Ω coax in analog form.

For the purpose of Power Monitor Interface, the LS also receive a digital signal representing the absolute optical power of the laser light on the optical bench.

5.5.2 Baseline design

The current baseline design involves two independent Nd:YAG laser sources on board each LISA s/c, denoted LO1 and LO2. These are operated at slightly different frequencies, where the frequency difference on the order of a few MHz is stabilized to the USO reference. Each of the independent laser oscillators is delivered to its respective optical bench on the SC with a polarization-maintaining, single-mode fiber. A summary of requirements for the laser system is given in Table 5.5-1.

Quantity	Requirement	Comment
Laser wavelength	1064.57 nm ± 1GHz	Nd:YAG NPRO oscillator anticipated
Power delivered to OB (end of life)	1200 mW	Based on current OB layout
RIN noise	$10^{-3}/\sqrt{\text{Hz}}$, $1/f^2$ rolloff below 1 mHz	After power stabilization
Frequency stability	$30\frac{\text{Hz}}{\sqrt{\text{Hz}}}\times\left[\left(\frac{0.1\text{Hz}}{f}\right)^{1.5}+\frac{1}{1+\frac{f}{100\,\text{Hz}}}\right]$ for frequencies between 30 μHz and 20 kHz.	as provided by stand alone LS
External Frequency Stabilization	100 kHz BW ±10 MHz range	For frequency stabilization by Phase Measurement System
Polarization linearity	98%	at fibre exit
PN Code Modulation	1 MHz chip rate, 1% of total optical power	Signal generated by PMS
USO Modulation	8 GHz pure sine tone, 15% of total optical power	Signal generated by PMS

Table 5.5-1: Summary of preliminary requirements for the laser system.

Figure 5.5-3 illustrates the current baseline architecture of the LISA Laser Subsystem and indicates/clarifies implementation aspects. It is based on a so-called Master Oscillator Fiber Power Amplifier (MOFPA) approach, which combines several advantages relevant in this context.

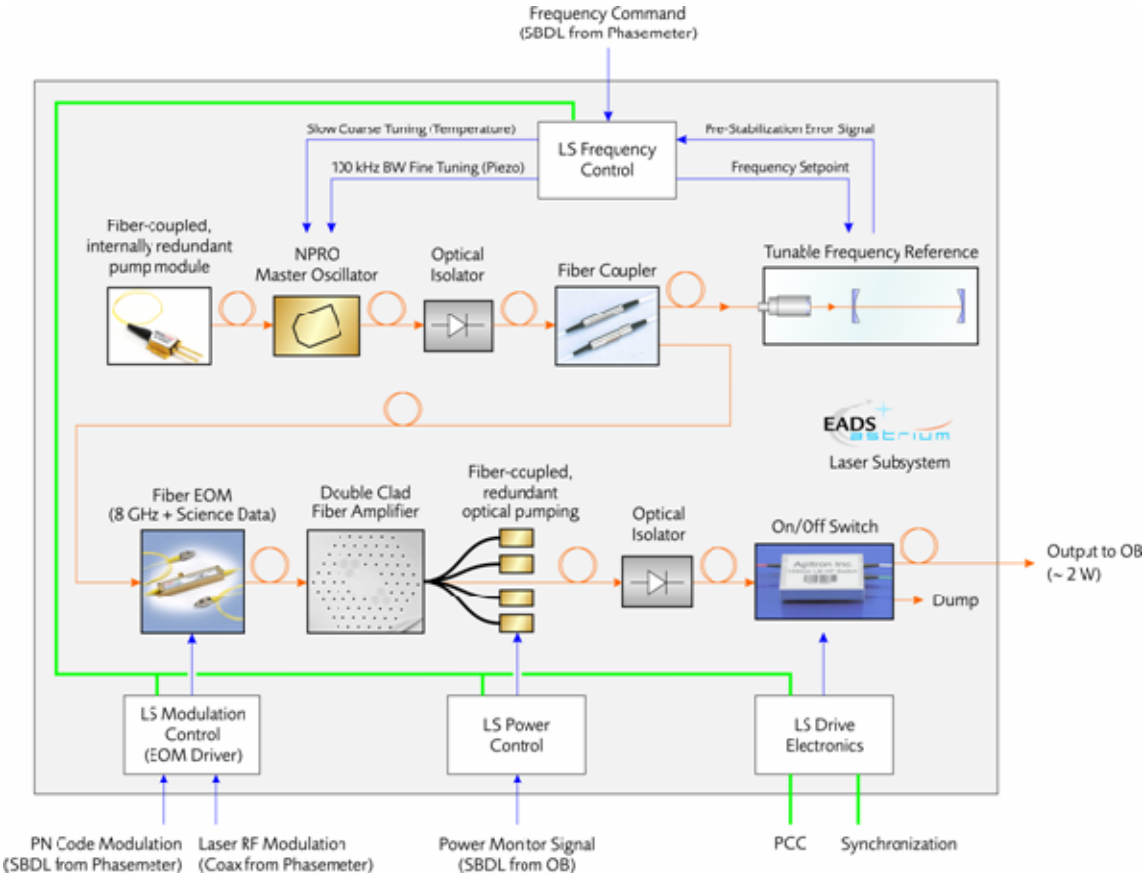

Figure 5.5-3: *LISA Laser Subsystem baseline architecture.*

A so-called Nd:YAG Non-Planar Ring Oscillator (NPRO) is utilized as master oscillator, which is proven to have excellent free-running spectral properties, hardly challenged by any other laser type. Part of its output is fed into a tunable frequency reference for pre-stabilization. The exact realization of the frequency reference is open so far, but the following alternatives seem to be the most attractive:

- Optical reference cavity with adjustable length (e.g. by piezo tuning).
- Sideband locking to a fixed length cavity, with adjustable sideband frequency.
- Unequal armlength interferometer using the standard LISA phase measurement for error signal generation (LISA Pathfinder style frequency stabilization).

The OBC signal and the Frequency Command from the phasemeter are processed by the LS Frequency Controller to adjust the frequency reference to the desired setpoint. The error signal from the frequency reference is fed back to the NPRO, where a high bandwidth loop acts on a piezo straining the NPRO crystal, on top of which an integrator removes any DC components by adjusting the crystal temperature.

The major part of the NPRO output is coupled into a fiber electro-optic modulator, which accomplishes the PN Code and 8 GHz sine modulation in a single broadband device. At its output, a total optical power of about 30 mW must be available for final amplification to the required power level of about 2 W. The amplification is realized in a double-clad active fiber, which is pumped by a combined system of redundant,

fiber-coupled pump diodes. These pump diodes are utilized for power control through adjustment of the diode current. The amplifier system is protected from any back reflections by a subsequent optical isolator.

At the output of the LS, a fiber-coupled latching switch enables a quick, frequent, and hysteresis-free control between an on- and an off-state of the laser system, without the need to switch diode currents. Thus, the thermal environment and in consequence the spectral properties of the LS remain perturbation-free.

5.6 Diagnostics Subsystem

As described in chapter 4.2, there exist strong requirements against the environment in where the interferometer assembly shall work in. For later science data interpretation, it is of importance to have sufficient knowledge about the environment at the time the data was gathered. Also, for in orbit testing and performance evaluation, it is desirable to have dedicated sensors and stimulators - these are summarised in the Diagnostics Subsystem.

Magnetic coils in close proximity to the GRS heads will be used to stimulate forces on the proof mass. The GRS system answer will be used to validate performance/sensitivity and set technical parameters. A magnetometer will be used to observe magnetic field forces such that EM-field changes can be detected and root cause analysis can start. For thermal condition stimulation and observation, heaters and highly accurate thermal sensors (thermistors) will be used. Their physical placement is matter of later, detailed thermal analysis, which will dictate optimal temperature reference points (TRP) and stimulation points.

A pressure transducer (type TBD) will measure the quality of the vacuum around the GRS head. This information can be enable the decision on ground for venting the GRS head - when the outer vacuum will provide vacuum better than 10^{-5} Pa.

The gathering of data of the radiation environment will help to analyse abnormal events and give indications about the real total dose all S/C equipments will see.

Some of the describe equipments will be found rather numerous on the payload or the spacecraft. They all will be driven by a single electronics box, specialised for the purpose of analogue signal readout and high accurate power supply. This box will house the Diagnostics Drive Electronics (DDE) which will also be equipped with a communication bus interface and act as a packet terminal. TM and TC will be send/received by this unit and internally process such that the desired components will be actuated accordingly and TM data will be gathered.

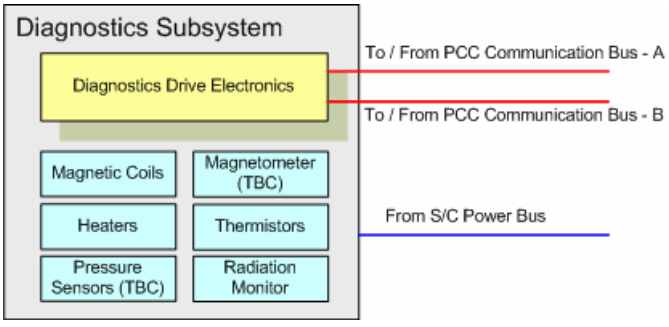

Figure 5.6-1: *Functional Breakdown of the Diagnoistics Subsystem*

6 Abbreviations

This section includes a list of abbreviations used throughout this document.

Acronym	Description
AC	Alternating Current
AIV	Assembly Integration & Verification
AOCS	Attitude and Orbit Control System
ASD	Astrium GmbH
ASU	Astrium Ltd
AU	Astronomic Unit
BW	Bandwidth
CCD	Charge-coupled Device
CCU	Caging Control Unit
CDH	Command and Data Handling
CFRP	Carbon Fibre Reinforced Plastic
CM	Caging Mechanism
CPDU	Command Pulse Distribution Unit
CTE	Coefficient of Thermal Expansion
DAC	Digital Analogue Converter
DC	Direct Current
DFACS	Drag Free Attitude & Control System
DH	Data Handling
DOF	Degree of Freedom
DP	Diagnostics Package
DWS	Differential Wavefront Sensing
EH	Electrode Housing
EMC	Electro-Magnetic Compatibility
EOM	Electro-Optical Modulator
FDIR	Failure Detection and Recovery
FEE	Front-End Electronics
FEEP	Field Emission Electric Propulsion
FSU	Fibre Switching Unit
FSW	fibre switch
GRS	Gravity Reference Sensor
GRSH	GRS Heads
HDRM	Hold Down and Release Mechanism
HGA	High Gain Antenna
ICD	Interface Control Document
IM	Isostatic Mount
IMU	Inertial Measurement Unit
IR	Infrared
ISL	Inter Spacecraft Link
IWS	Inertial Wavefront Sensor
LEOP	Launch and Early Orbit Phase
LGA	Low Gain Antenna
LISA	Laser Interferometer Space Antenna
LLD	Launch Lock Device
LNA	Low Noise Amplifier

LO	Laser Optics
LOS	Line of Sight
LPF	Lisa Pathfinder
LPS	Laser prestabilisation subsystem
LS	Laser Subsystem
LTP	LISA Technology Package
MBW	Measurement Band Width
MDR	Mission Design Review
MGSE	Mechanical Ground Support Equipment
MOFPA	Master Oscillator Fiber Power Amplifier
MOSA	Moving Optical Subassembly
MRD	Mission Requirements Document
MTR	Mid-Term Review
NEI	Noise-equivalent intensity
NPRO	Non-Planar Ring Oscillator
OA	Optical Assembly
OAE	Optical Assembly Electronics
OAM	Optical Assembly Mechanics
OAME	Optical Assembly Mechanism Electronics
OAS	Optical Assembly Subsystem
OATM	Optical Assembly Tracking Mechanism
OB	Optical Bench
OBC	On-Bord Computer
OGSE	Optical Ground Support Equipment
ORO	Optical Readout
PAAM	Point Ahead Assembly Mechanism
PCDU	Power Control and Distribution Unit
PCS	Payload Control System
PM	Proof Mass
PMDSP	Phase Measurement Digital Signal Processor
PMFDE	Phase Measurement Frequency Distribution Electronic
PMFEE	Phase Measurement Front End Electronics
PMS	Phase Measurement System
QPD	Quadrant Photo Diodes
RD	Reference Document
ReM	Refocussing mechanism
RF	Radio Frequency
RFDU	Reference Frequency Distribution Unit
RIU	Remote Interface Unit
RMS	Root Mean Square
RSS	Root Sum Square
SAU	FEE Sensing and Actuation Units
SC	Spacecraft
SNR	Signal to Noise Ratio
STR	Star Tracker
TBC	to be confirmed
TBD	to be defined
TC	Thermal Control
TM	Telemetry
TN	Technical Note

TS	Telescope Subsystem
TX	Transmission
ULU	UV Light Unit
USO	Ultra Stable Oscillator
UV	Ultraviolet